CHARACTERIZATION OF *XIPHOPHORUS MACULATUS* POLYMERASE β CONTAINING A SITE DIRECTED MUTATION AT ASPARTIC ACID 63

THESIS

Presented to the Graduate Council
of Texas State University-San Marcos
in Partial Fulfillment
of the Requirements

for the Degree

Master of SCIENCE

by

Douglas Barth, B.S.

San Marcos, Texas
August 2006

ACKNOWLEDGEMENTS

I would like to take the time to thank Dr. Walter for allowing me to work in his research group at Texas State University-San Marcos and for providing a position in his laboratory during my time as a graduate student. Dr. Walter provided me with guidance while being patient as I continued to learn.

I would also like to thank both Dr. Lewis and Dr. David for their encouragement and for taking the time to answer any questions that I had.

Finally, I would like to thank the molecular bioscience research group for their help and willingness to offer their own time to help me learn.

This manuscript was submitted on May 28, 2006.

TABLE OF CONTENTS

LIST OF FIGURES

LIST OF TABLES

CHAPTER 1

INTRODUCTION

DNA polymerase β (Polβ) is involved in DNA replication and repair. Mammalian Polβ is a 39 kDa protein comprised of 335 amino acids. Polβ is classified as a type X enzyme, part of the terminal transferase family [1]. The structure of Polβ has been determined and is often described as a hand motif containing two sub-domains dubbed fingers and thumb (Figure 1-1). The activity of purified Polβ is measured using dsDNA substrates possessing a single nucleotide gap (Figure 1-2). The 31 kDa thumb domain is responsible for the nucleotidyl transferase activity of Polβ, while the 8 kDa finger domain contains the deoxyribose phosphate lyase activity [2, 3]. Polβ lacks exonuclease activity [4]. The small size of the protein combined with a relatively simple bi-functional activity makes Polβ a very good target to study general polymerase enzymology.

The Polβ structure allows binding of both a single nucleotide triphosphate and a double-stranded DNA (dsDNA) molecule containing a single nucleotide gap; as long as the gap provides a 3′-hydroxyl residue (i.e., template primer substrate). Evidence suggests that before the catalytic function of human Polβ can proceed, nonspecific and non-covalent binding of the DNA molecule to a single nucleotide triphosphate (dNTP) must occur [5]. Initial binding of the enzyme is thought to occur via non-covalent interactions of the nucleotide 5′-phosphate in the gap with the Polβ finger domain [3, 5]

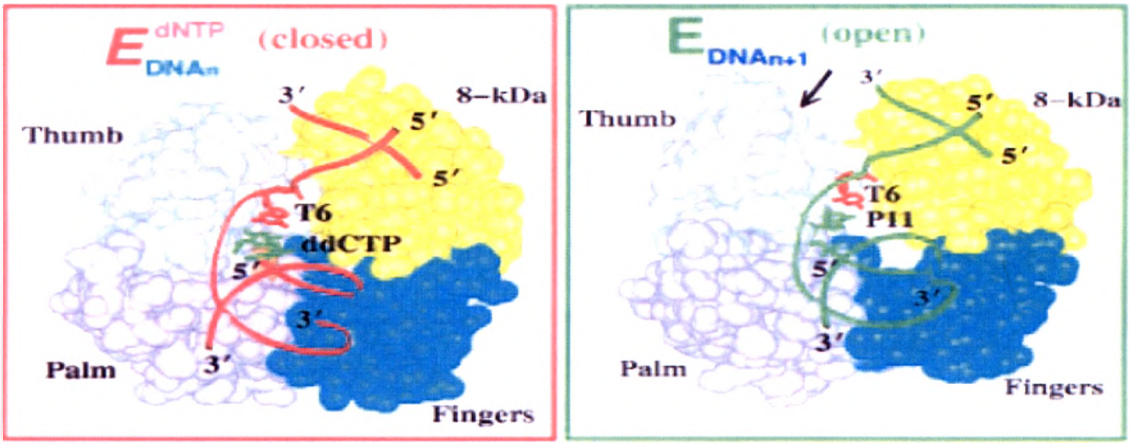

Figure 1-1 – Human Polβ Binding DNA in Closed and Open Conformations [6].

A space filling molecular image of human Polβ as deduced by X-ray crystallography depicts two domains of the protein. The 8 kDa "finger" domain is shown as yellow, whereas the 31 kDa "thumb" is shown as blue. This image shows both states of the enzyme, closed and open. The closed state occurs after the complexation event, but prior to catalytic insertion of the nucleotide. The open state represents a time either before nucleotide insertion or in this case just before the substrate is release. Also shown is positioning of the DNA strand and nucleotide triphosphate during both the open and closed states. [Schlick and Radhakrishnan, 2004]

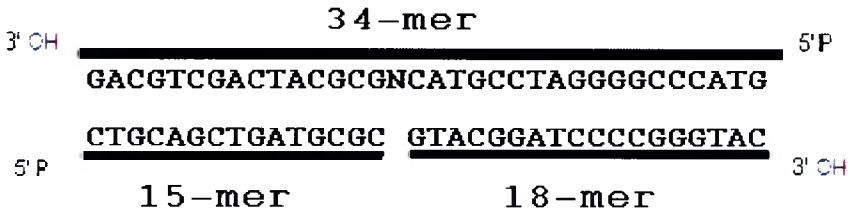

Figure 1-2 – "Gapped" DNA Template.

Example of double stranded DNA with a single nucleotide gap that acts as substrate for Polβ. The N represents the nucleic acid template for nucleotide insertion.

(Figure 1-3). In this scenario, lysine 68 (within the thumb domain) is thought to interact in a dehydration reaction with the 5′-deoxyribose phosphate at the C1 position forming a Schiff base intermediate [5]. The Schiff base formation is followed by β-elimination completing the dRP lyase activity [5]. The DNA binding event induces conformational change in the enzyme that involves rotation of the finger domain to complete a grasping type motion of the template dsDNA strand.

After binding of the Polβ enzyme to the substrate, a 90° kink is observed at the 5′-phosphodiester bond of the template DNA strand [4]. The closed hand conformation stabilizes this structure and allows the reaction to proceed (Figure 1-4). Six key residues within the active site have been implicated in hydrogen bonding involved in coordination of the nucleotide and the DNA/enzyme complex: Arg 283, Phe 272, Asp 190, Asp 192, Tyr 271, and Asp 256 [3, 5, 6]. After orientation of the enzyme on the nucleic acid substrate, a phosphodiester bond is formed between the α-phosphate of the triphosphate nucleotide and the 3′-phosphate of the gapped DNA strand, filling the single nucleotide gap in the DNA molecule (Figure 1-5). The phosphodiester bond is thought to form via coordination by two metal ions [7]. Initially the 3′-hydroxyl makes a nucleophilic attack upon the α-phosphate of the mononucleotide [3]. Two metal ions that coordinate this attack are held in place by residues Asp 256, Asp 190, and Asp 192 [6]. One of the metal ions holds the 3′-hydroxyl of the DNA strand in place while the other forms a tridentate moiety with the phosphate groups in the dNTP [5,6]. This positioning moves the dehydrogenated hydroxyl 180° away from the oxygen linkage of the α and β phosphate of the incoming dNTP [6]. Such exact positioning is crucial for nucleophilic attack to occur. The reaction leaves a nick on the 3′ side of the incorporated nucleotide and

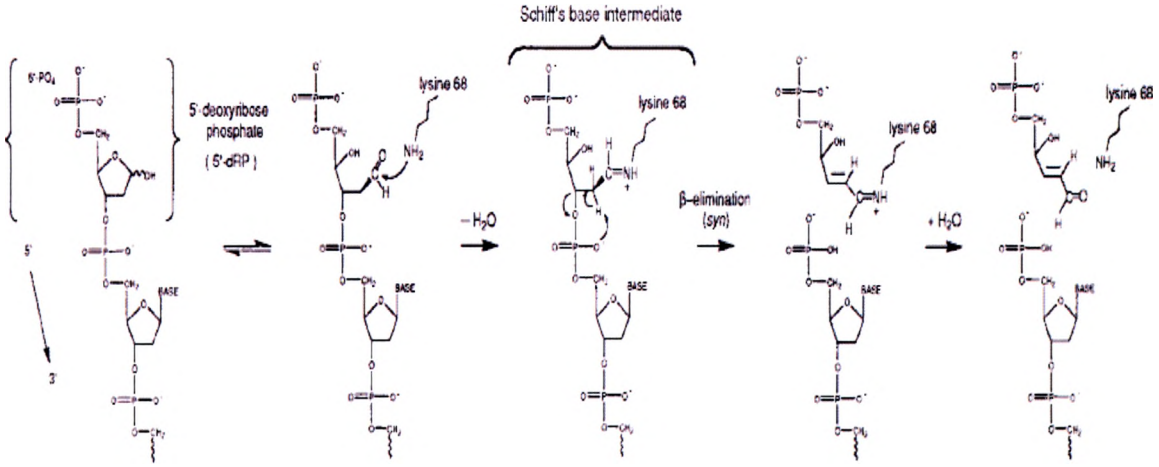

Figure 1-3 - Proposed Mechanism for dRP Lyase Activity of Human Polβ [5].

The initial binding of the enzyme to the dsDNA molecule is thought to be through interactions of the lysine 68 residue. Formation of a Schiff base intermediate is the result of the interaction. The reaction results in the formation of the DNA substrate with the single nucleotide gap. [Sawaya et al., 1997]

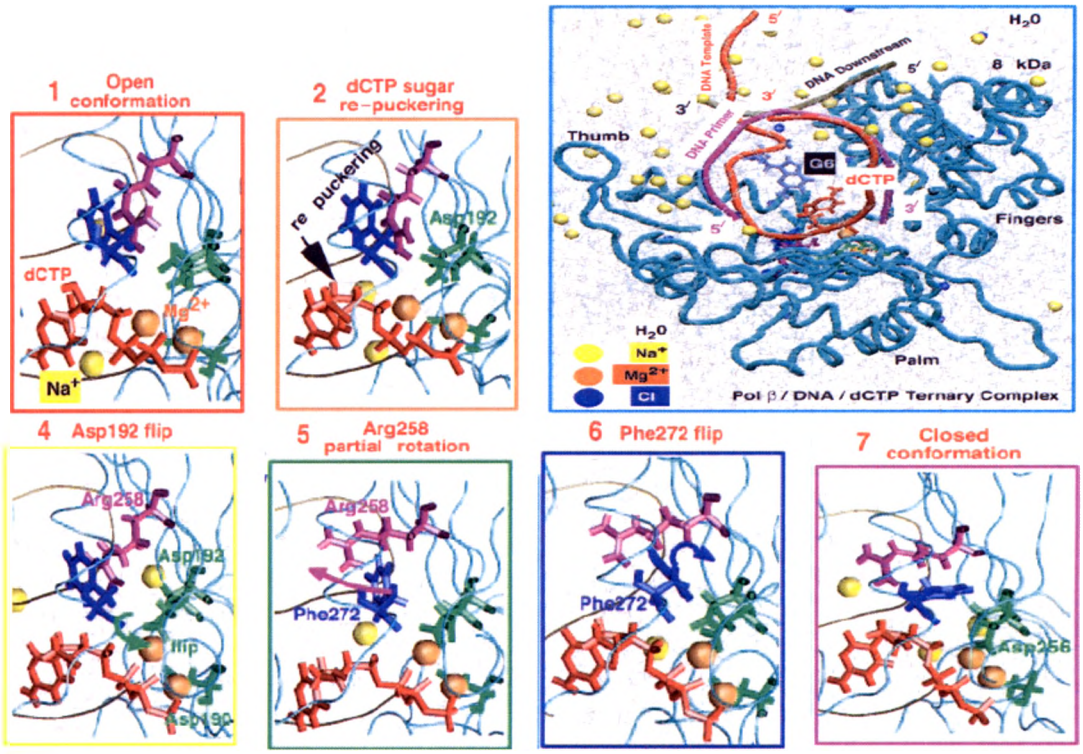

Figure 1-4 - Nucleotide Positioning and Conformational Change of Human Polβ [6].

The conformational change within polβ has been suggested to play a role in nucleotide selection. Figure 1-4 shows seven intermediate steps proposed between the open and closed states of Polβ. The red stick model represents a dCTP being inserted into the gap across from the GTP nucleotide, seen in model 3 in blue. Residues perceived as active in active site positioning are contained within the "thumb" domain. First, the open formation is disturbed upon the free nucleotide entrance into the active site. Second, the nucleotide is puckered upon interaction with the metal cofactor. Third, the formation of a 90° kink in the DNA molecule is observed. Fourth, a flip of Asp 192 is deduced. Fifth, a partial rotation of Arg 258 is proposed. Sixth, a flip of Phe 272 is deduced. Upon enzyme closing the metal cofactors realign in position forming a tridentate moiety with the free nucleotide. [Schlick and Radhakrishnan, 2004]

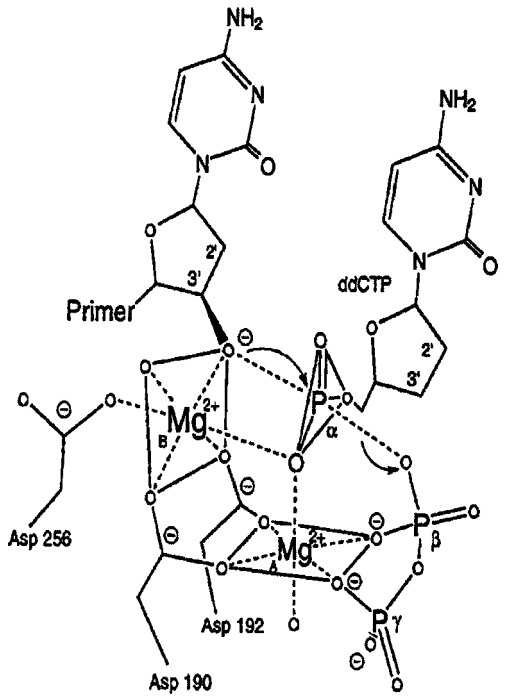

Figure 1-5 - Proposed Nucleotidyl Transfer Mechanism of Human Polβ[5].

Nucleotide transfer is arranged through the coordination of a tridentate moiety of the incoming nucleotide triphosphate group with magnesium. The magnesium cofactors are proposed to be aligned via coordination with Asp 190, Asp 192, and Asp 256. Formation of a phosphodiester bond occurs when the 3' end of the primer binds to the incoming dCTP nucleotide. Positioning of both the dsDNA substrate and the incoming nucleotide is favorable for the nucleophilic attack to occur. [Sawaya et al., 1997]

releases pyrophosphate. The human Polβ has been proposed to possess a mechanism that has been dubbed an "induced fit" mechanism. An induced fit mechanism describes the relationship of the inclusion of both the template and the free nucleotide prior to enzymatic activity. Three stipulations must be met to be an "induced fit" [8]. One, the existence of two conformations of the active site, both an active state and inactive state, must occur. Two, there should be a conformational change triggered by base pairing of the free nucleotide with the template. Three, there must be selectivity between correct and incorrect base pairing that serves to trigger the enzymatic activity. There has been some debate over whether this accurately describes the Polβ mechanism. Alternative mechanisms include either a model here the Polβ acts simply to polymerize the phosphodiester bond in the backbone of the DNA molecule in a non-discriminating way as though it were a "zipper" or some yet to be explained mode of operation.

Polβ acts nonexclusively in base excision repair (BER) pathways ("short patch" BER and "long patch" BER) filling gaps in the DNA molecule (Figure 1-6). BER pathways serve to protect genomic stability by allowing damaged bases to be removed and correct bases inserted. BER pathways are required to fix over 10,000 damaged bases per day within a normal mammalian cell [9, 10]. Base damage may be due to spontaneous oxidation, deamination, alkylation, depurination, or other chemical processes. In addition to spontaneous damage, environmental agents may also produce modified bases or DNA adducts. In single nucleotide BER (Figure 1-6), a glycosylase removes the damaged purine or pyrmidine from the deoxyribose backbone. The created Ap (apurinic/apyrmidinic) site is then nicked on the 5′ side of the AP site by AP endonuclease. Polβ may both remove the 5′ deoxyribose phosphate and replace the

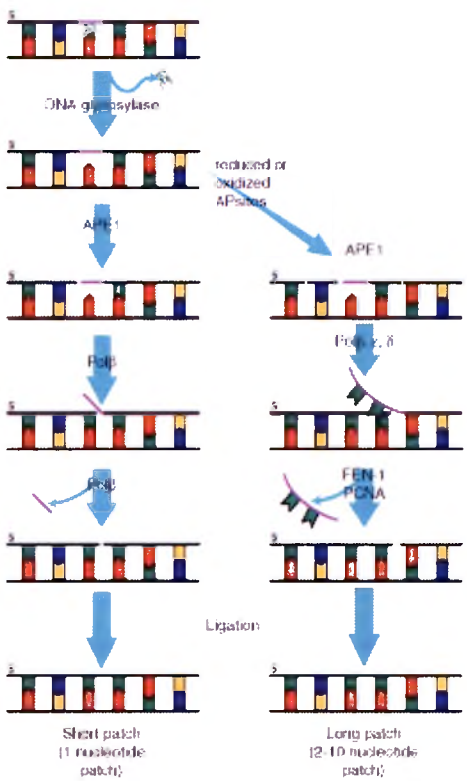

Figure 1-6 - Base Excision Repair Pathway.

"Short patch" and "long patch" BER pathway both start with the recognition of DNA damage and removal of the damaged base by a glycosylase. In "short" patch repair AP endonuclease (APE) nicks the abasic site. Polβ then coordinates nucleotide incorporation while cleaving the dRP using its lyase activity. DNA ligase completes the pathway by sealing the nick. "Long" patch repair is undertaken when the abasic site is reduced or oxidized. This difference prevents ligation and induces a protein complex to be formed. This complex including both a polymerase and PCNA can replace up to 10 nucleotides. Removal of the "flap" is performed by FEN-1 and is followed by ligation via DNA ligase. [*http://www.rndsystems.com/DAM_public/5171.gif*]

single nucleotide gap in the DNA. DNA ligase is required to seal the nick after the inserted nucleotide.

"Long patch" repair (Figure 1-6) begins with a glycosylase removal of the damaged base. The resulting abasic site is then nicked by Apurinic/Apyrmidinic (Ap) Endonuclease (APE). The inability of Polβ to remove a 5′-deoxyribose phosphate because of interstrand damage is thought to force multiple bases to be displaced [9, 11]. Insertion of nucleotides may be carried out by Polβ or Polymerase ε and Polymerase δ in conjunction with Proliferating Cell Nuclear Antigen (PCNA) [14]. The polymerase acts on the gap in the DNA strand with the aid of PCNA. The repair complex synthesizes a 2 to 10 nucleotide stretch of DNA. This process leaves a "flap" that has been suggested to be cleaved by Flap Endonuclease (FEN-1). "Long patch" BER ends when DNA Ligase seals the nick 3′ to the inserted nucleotide. The net effect of BER is to ensure genome maintenance and stability. The fidelity of Polβ in BER refers to the accuracy in selection of the correct nucleotide to complement the template DNA strand.

The function of Polymerase β within the BER pathway is insertion of the correct nucleotide into a gap formed by the removal of a damaged base. BER in mammalian cell-free extracts results in base substitution error frequencies ranging from 5.2 - 7.2 x 10^{-4} [10]. As previously stated, Polβ is not the only polymerase involved in BER. Human Polβ has been shown to possess base substitution error rates ranging from 0.3 - 2.8 x 10^{-4}, when acting on a single nucleotide gapped substrate [11]. The fidelity of Polβ has been shown to increase several fold upon the addition of other proteins (Ap Endonuclease, PCNA, FEN-1, and/or DNA Ligase) known to be involved in BER [11, 12, 13, 14, 15].

A study using POLβ-null mutant mice (POLβ -/-) reports both growth retardation

and respiratory failure 15 minutes after Caesarin section birth 18.5 days after conception [16]. Polβ-deficient mice were not found at post-natal day one [16, 17]. The dissection of embryos, that were acquired three weeks after conception, revealed apoptosis of post-mitotic neuronal cells [16]. Mosaic models that maintain a state of Polβ deficiency (contains cells of Polβ +/- and Polβ -/-) were reduced in weight and size [16]. Most Polβ-deficient mosaic mice do not survive initial stages of development [16]. This observation indicates that mouse polβ is an essential enzyme for normal development.

Polβ has been studied across many eukaryotic organisms. Polβ experimentation in zebrafish, *Xiphophorus*, frogs, chickens, rats, and humans have studied topics including gene structure, transcriptional patterns, protein structure, enzymatic activity, and enzyme function. Studies across this broad spectrum of species have been undertaken for comparative analyses.

Xiphophorus are a small live bearing fish consisting of 26 tropical species. *Xiphophorus* serve as biomedical aquaria models of induced and spontaneous carcinogenesis [18, 19, 20]. Compared with other experimental models, the *Xiphophorus* tumor models have many benefits; the ability to produce large numbers of tumor-bearing animals, well-defined genetics, phenotypically diverse parents, and cancer induction mechanisms that correspond to carcinogenesis in humans [18]. A well studied spontaneous tumor model, termed the "Gordon-Kosswig" melanoma model, involves backcross of *X. maculatus* (x) *X. helleri* interspecies F_1 hybrids with the *X. helleri* parental line (Figure 1-7) [19]. In this case, 25% of the backcross hybrid progeny develop melanoma. A sex-linked pigment pattern termed *Sd* (spotted dorsal) is implicated in melanoma formation [19]. The "Gordon-Kosswig" model has been used to

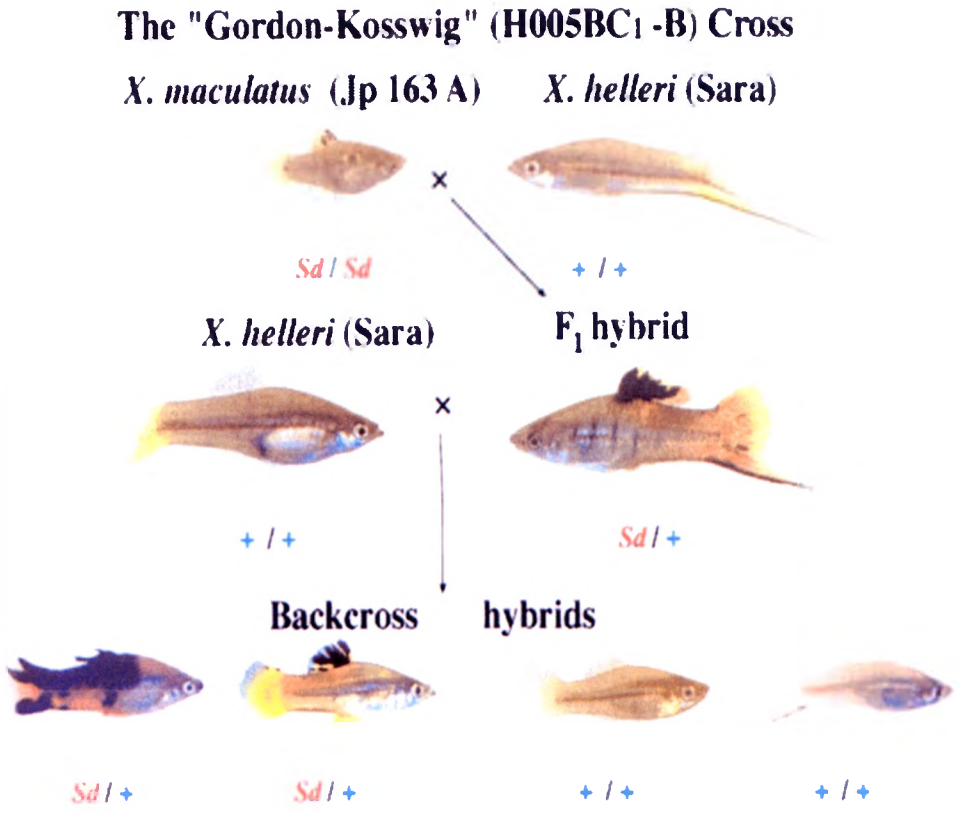

Figure 1-7 - *Xiphophorus* Gordon-Kosswig Melanoma Model.

The *X. maculatus* (Jp 163 A) is mated with the *X. helleri* (Sarabia) to form an F_1 interspecies hybrid. The F_1 hybrid is then mated with the *X. helleri* to produce the backcross hybrids. 25% of the BC_1 progeny (dark pigment patterned, bottom left) develop melanoma.

identify gene candidates associated with spontaneous melanoma development [19]. Unlike the "Gordon-Kosswig" spontaneous melanoma model, several other *Xiphophorus* interspecies tumor models have been shown to develop tumors only after induction by treatment of young backcross hybrid fish with DNA damaging agents such as ultraviolet light (UVB) or methylnitrosourea (MNU) [19, 20]. Retinoblastoma, neuroblastoma, fibrosarcoma, rhabdomyosarcoma, schwannoma, and melanoma have all been shown to result from UVB or MNU induction of select *Xiphophorus* interspecies backcross hybrids [20, 21, 22]. Polβ is an enzyme present within the cell that has the ability to participate in repair of damaged DNA upon tumor induction treatment.

Xiphophorus Polβ (*X*polβ) consists of 337 amino acids and is also 39 kDa [23]. A comparison of *X*polβ to human Polβ shows 46 non-identical amino acids (Figure 1-8). There are 23 non-conservative differences in the primary sequences of *X*polβ and human Polβ. The primary structure of the protein contains 89% amino acid similarity when compared with the human form (Figure 1-8). Initial studies of *X*polβ have shown enzymatic activity to be within observed values reported for human Polβ activity [23].

*X*polβ contains an aspartic acid at position 63 within the thumb domain human Polβ amino acid 63 is proline. In human Polβ, residues 62 through 64 form a hairpin secondary structure that is part of a helix-hairpin-helix (HhH) motif (Figure 1-9). This hairpin is highly conserved among mammalian forms of the protein. The properties of proline suggest that the hairpin structure is in large part due to proline 63. Residue 63 is also four amino acids upstream from an active residue in initial DNA binding, lysine 68.

The serine 79 residue in human Polβ is located between HhH motif 1 and HhH motif 2 in the 8kDa domain [24]. Using site directed mutagenesis, a T79S mutant human

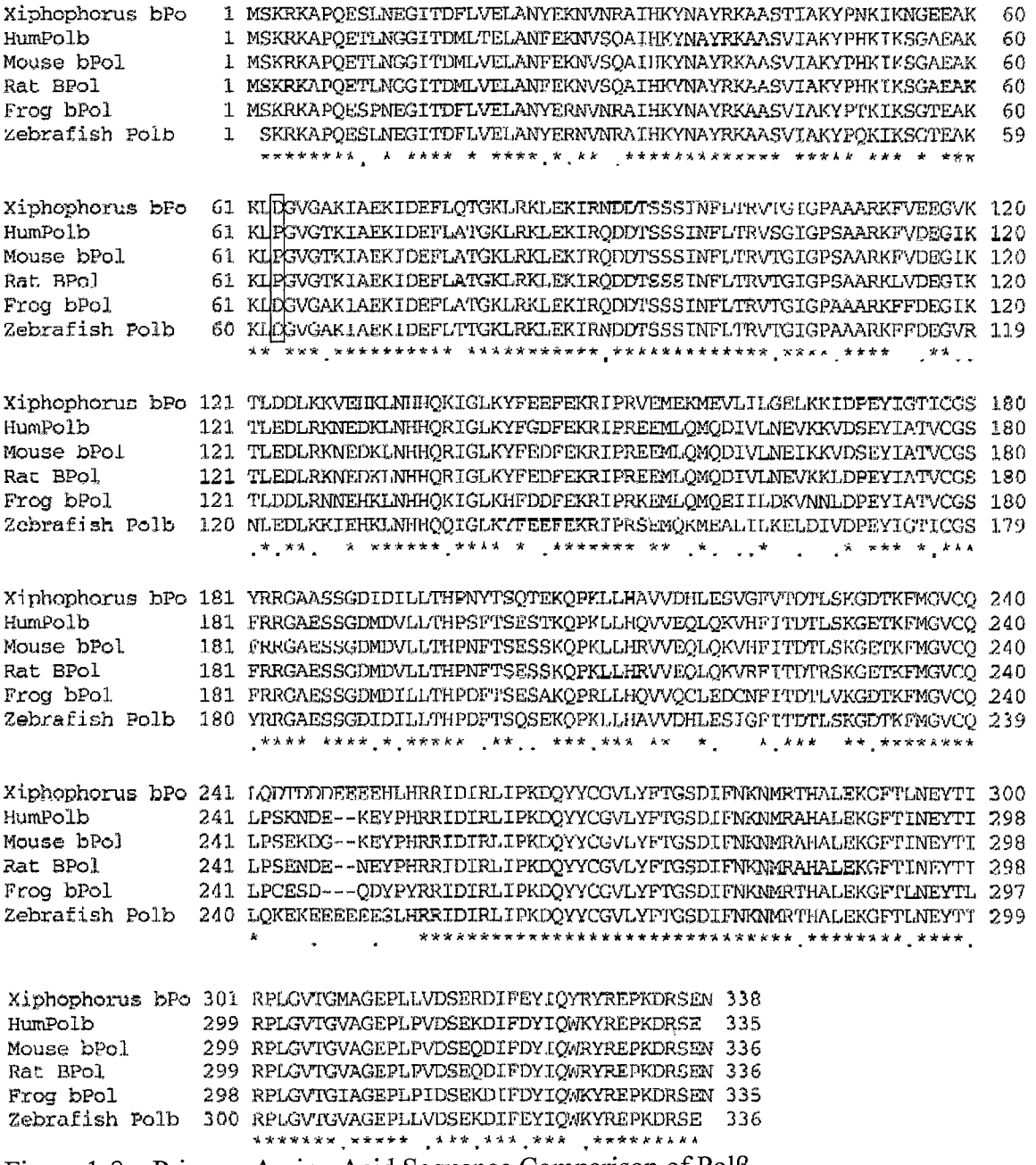

Figure 1-8 – Primary Amino Acid Sequence Comparison of Polβ.

The amino acid sequences of six vertebrate Polβ proteins are displayed for comparison of the primary sequences. The frog, zebrafish, and Xiphophorus proteins all contain an aspartic acid residue at position 63 while mammals contain proline. Identical amino acids are denoted with an asterisk. Similar amino acids are denoted with a period.

polβ protein was shown to exhibit an 8-fold increase in spontaneous mutation frequency [24]. Site-directed mutagenesis of aspartic acid 63 to proline (D63P) within the *Xiphophorus* Polβ protein may be expected to result in a change in mutation frequency due to location of this amino acid within a hairpin of the HhH motif in the finger domain. *X*polβD63P is to be translated from the *Xiphophorus* cDNA sequence after the sequence is altered using site-directed mutagenesis. Site-directed mutagenesis will be used to change the cDNA sequence at codon 63. The change of the codon will be translated into the amino acid proline at location 63 of the primary *Xiphophorus* amino acid sequence. In this study we will examine the *X*polβD63P effect upon the fidelity of the *X*polβ enzyme via steady state kinetic analyses.

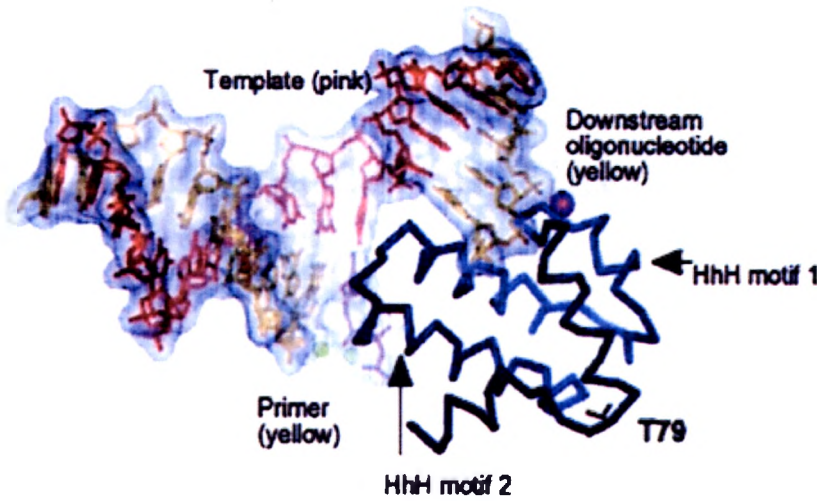

Figure 1-9 - Helix-Hairpin-Helix Motifs Contained in Human Polβ [21].

Two helix-hairpin-helix (HhH) motifs are present within the finger domain of polβ. In the HhH motif 2 (black), the thoeronine 79 residue is located between the two HhH motifs. Proline 63 is located within the hairpin of HhH motif 1 (blue). Figure 1-9 displays how this area of the protein interacts with the DNA template. [Maitra et al., 2001]

CHAPTER 2

METHODS AND MATERIALS

Xiphophorus Stock Center

Mature male *Xiphophorus maculatus*, of the highly inbred Jp 163 A strain, were used as the source for the *X*POLβ cDNA. All fish were obtained from the *Xiphophorus* Stock Center, Texas State University, San Marcos, Texas. (see www.xiphophorus.org)

Coding Sequence and Expression Plasmid

The *Xiphophorus* POLβ coding sequence was previously cloned in our laboratory from the *Xiphophorus maculatus* Jp 163 A brain cDNA [23]. Plasmid p*Xiph*polβ contains the entire open reading frame of the wild-type *Xiphophorus maculatus* POLβ gene [23]. Plasmid p*Xiph*polβ was purified for use in the pET100/D-TOPO vector recombinant protein expression system (Invitrogen, Carlsbad, CA). The pET100/D-TOPO plasmids encode a start codon, a poly-His tag, an Anti-Xpress™ epitope and an enterokinase cleavage site. The complete open reading frame for *X*POLβ was PCR amplified from p*Xiph*polβ using a forward primer with CACC immediately in front of the coding sequence and a reverse primer containing a stop codon prior to insertion into the pET vector. The resulting PCR products were analyzed by gel electrophoresis and a

1,212 base pair band was extracted and purified from the gel matrix. The purified product was ligated into the pET vector via a reaction using topoisomerase to hybridize the CACC with the GGTG overhang on the pET100/D-TOPO vector. This produced the plasmid p*Xiph*Polβ #6 that harbored the *Xiphophorus* polβ gene. Archived bacterial cell cultures containing the p*Xiph*Polβ #6 vector construct were stored at -80°C.

Site-Directed Mutagenesis

Site-directed mutagenesis was carried out using the QuikChange Multi Site-Directed Mutagenesis Kit (Stratagene Inc., La Jolla, CA). The plasmid p*Xiph*Polβ was used as a target for polymerase chain reaction (PCR) with phosphorylated primers containing the desired mutation. Primer extension reaction was carried out using *pfu*Turbo DNA polymerase, 10x reaction buffer (1M potassium acetate, 250mM tris-acetate [pH 7.6], 100mM magnesium acetate, 5mM β-mercaptoethanol, 100μg/ml BSA), p*Xiph*Polβ (100ng), dNTP mix (25μM), and using a single 5'-phosphorylated primer, polβ-P63 (5'-GAGAAGAGGCGAAGAAACTGCCGGGAGTTGGTG-3') (100ng). DNA isolated from *E. coli* cells is typically dam methylated. *Dpn*I digests both methylated and hemimethylated DNA and was used to digest the parental DNA template. A 1,212 bp PCR product was isolated from agarose gels and digested with *Dpn*I (10 units) for 1 hour at 37°C. Transformation of XL10-Gold ultracompetent *E. coli* cells was achieved with 4μl DpnI restricted DNA. The transformation reaction was allowed to incubate for 30 min on ice before heat shock at 42°C for 30 seconds. The transformed cells were then placed in 500μL of SOC medium (20g tryptone, 5g yeast extract, 0.5g NaCl, 20mM glucose) and incubated at 37°C for 1 hr. After incubation, *E. coli* cells were plated onto LB media (5g Tryptone, 2.5g Yeast Extract, 5g sodium chloride, 7.5g

Table 2-1

Oligonucleotides Used in Site-Directed Mutagenesis.

Oligonucleotides used in site-directed mutagenesis

PolβF5 – Polβ pET insertion sequence forward primer

5' CACCATGAGCAAGAGGAAAGCTCCAC 3'

PolβR2 – Polβ complete coding sequence reverse primer

5' CCATGTTTGCAGGACTGCTGT 3'

Polβ-P63D – Polβ site-directed mutagenesis coding sequence primer

5' GAGAAGAGGCGAAGAAACTGCCGGGAGTTGGTG 3'

All primers were purchased from Intergrated DNA Technologies (Coralville, IA)

Bacto Agar, 30mg Ampicillin, 36mg X-gal). Colonies from the LB media were selected and grown overnight in 10mL of tryptone broth (5g tryptone, 2.5g yeast extract, 5g sodium chloride). Cell cultures were centrifuged at 7,000 x g to isolate the cells and the cell pellets were resuspended in 250µl of purification buffer 1 (0.1µg/mL RNase I), then lysed in 200µl of purification buffer 2 (2.5% sodium dodecylsulphate, 1% sodium hydroxide). Three hundred and fifty µl of neutralizing buffer (40% guanidine hydrochloride, 20% acetic acid) was added to the cell lysate. Cellular debris was removed via centrifugation at 17,900 x g and supernatant collected. Cell lysate supernatant was filtered in a QIAprep spin column (Qiagen Inc., Valencia, CA). DNA was eluted through the column by addition of 50µL of elution buffer (10mM Tris-HCl, pH 8.5, 65°C). The isolated DNA was sent for nucleotide sequencing of the complete insert (Davis Sequencing, LLC., Davis, CA). Selected colonies that contained the desired site-directed mutation were designated p*X*polβD63P and stored at -80°C in 50% glycerol.

Protein expression and protein purification

Archived expression vectors containing the desired coding sequences were grown overnight at 37°C. Plasmids p*X*polβD63P and p*Xiph*Polβ #6 were isolated as described previously and used to transform BL21Star (DE3) *E. coli* cells (Invitrogen, Carlsbad, CA). Cell cultures were grown in 500mL of tryptone broth (5g tryptone, 2.5g yeast extract, 5g NaCl). Cell cultures were grown overnight at 37°C. Cell cultures were then induced for gene expression for 2-4 h by the addition of 1mM isopropyl-β-D-thiogalactoside (IPTG). Cells were harvested by centrifugation (3000 x g, 15min) and stored at -80°C.

Cell pellets were resuspended in 10mL of the native purification buffer (50mM sodium phosphate pH 8, 500mM NaCl, 1mg/mL lysozyme). Six pulses of bath sonication (Solid State/Ultrasonic FS-14, Fisher Scientific) for a duration of 15 seconds were used to break open the cells. Cell lysates were passed through an 18-gauge syringe to decrease the viscosity. Centrifugation of the cell lysates for 30 min at 3000 x g yielded soluble and insoluble (pellet) fractions. The soluble fraction was applied to a nickel-nitrilotriacetate-agarose (ion metal affinity chromatography) column (Invitrogen, Carlsbad, CA) for approximately one hour. The column was washed 4X with wash buffer (50mM sodium phosphate pH 8.0, 500mM NaCl, and 25mM imidazole). Then elution buffer (50mM sodium phosphate pH 8.0, 500mM NaCl, and 250mM imidazole) was added to remove bound protein from the column. The elutant was collected in eight 1mL fractions and each fraction was analyzed by sodium dodecyl sulfate polyacrylamide gel electrophoresis (SDS-PAGE). Fractions containing a protein band of approximate size of the N-terminal tagged *X*polβ protein were dialyzed against 50mM Tris-HCl pH 8.0, 1mM $CaCl_2$, 0.1% Tween 20 at 4°C. One mL suspension of purified fusion protein was digested with 25 units of enterokinase (EK, Invitrogen, Carlsbad, CA) overnight at 4°C to remove the fusion tag. EK was removed using a trypsin inhibitor-immobilized resin (EK-Away, Invitrogen, Carlsbad, CA). Recombinant protein samples were dialyzed against polβ storage buffer (50mM Tris-HCl pH 7.5, 200mM NaCl, 5% glycerol). Total protein concentration was determined using the Bradford assay. A dilution series was made from each sample and mixed with Coomassie blue reagent (0.2% coomasie G-250 dye, 50% methanol, and 7.5% phosphoric acid; Pierce, Rockford, IL, USA). A Power Wave (Bio-Tek Instruments, Winooski, VT) optical density plate reader was used to

determine the optical density of each dilution and the data compared to a standard curve of a BSA dilution established total protein concentration.

Western blot and SDS-PAGE

Collected protein samples from purification and EK digestion were analyzed using pre-cast Novex discontinous 4-12% Bis-Tris polyacrylamide gels (Invitrogen, Carlsbad, CA) run in a Xcell SureLock Mini-Cell (Invitrogen) gel rig. Five μL of the fractions were diluted into 20μL of NuPAGE LDS Sample Buffer (10% Glycerol, 141mM Tris base, 106mM Tris HCl, 2% LDS, 0.51mM EDTA, 0.22mM SERVA Blue G250, 0.175mM Phenol Red). The gels were run at 200 V for 30 to 45 min using NuPAGE MES SDS Running Buffer (50mM MOPS, 50mM Tris Base, 0.1% SDS, 1mM EDTA). Gels were washed and placed in a fixing solution (50% MeOH, 13% acetic acid) for 15 min then dyed with Comassie blue stain (Pierce) for approximately 30 min in order to visualize the proteins.

Western blots were initiated using a prestained gel placed within the XCell II Blot Module (Invitrogen). Transfer of protein from the prestained gel onto a nitrocellulose membrane occurred using the transfer buffer (25mM Bicine, 25mM Bis-Tris, 1.0mM EDTA, 0.05mM chlorobutanol) for 30 min at 30 V. The membrane was then probed with either Anti-Xpress™ antibody (Invitrogen, at 1:5000 dilution) or monoclonal mouse anti-polβ (Trevigen, at 1:2000 dilution) for up to an hour. Membranes were washed with antibody wash (concentrated saline solution containing detergent). A secondary antibody (alkaline phosphate-conjugated, affinity purified, antibody) was then applied for 30 min and the membrane again washed for 15 min in the antibody wash, followed by 5 min with

ddH_2O. Chemiluminescence substrate (CDP-Star chemiluminescent substrate with specificity for alkaline phosphatase) was pipetted across the surface of the membrane in order to detect the bound antibody (Western Breeze kit, Invitrogen). Gel images and Western blot analyses were captured and analyzed using a Kodak Digital Science Image Station 440CF in conjunction with Kodak 1D version 3.6.1 software (Eastman Kodak, New Haven, CT, USA).

Specific activity assay

The specific activity of both the wild-type *X*polβ protein and *X*polβD63P protein was determined by assay of the correct insertion of α-P^{32}-dATP into a single-nucleotide dT-gapped DNA substrate (Figure 1-2, Table 2-2). This incorporation reaction was performed with four concentrations of α-^{32}P-labeled substrate (2.5nM, 5nM, 10nM, and 20nM) at 15°C in 25μL containing 50mM Tris-HCl pH 8.0, 10mM $MgCl_2$, 20mM NaCl, 1mM DTT, 5% glycerol, 2μM single-nucleotide dT-gapped DNA substrate, and 10fmol of *X*polβ). The reaction sample was run through a vacuum filter apparatus and radiolabeled substrate collected on glass fiber discs (Whatman). The filter paper was washed with both ammonium formate and ethanol to force free nucleotide through the glass fiber disc and then allowed to dry. The glass fiber disc was submersed in 10mL of Scinti-Verse (Fisher Scientific, Fair Lawn, NJ) liquid scintillation fluor. Samples were then placed within a Beckman LS6000IC (Beckman, Fullerton, CA) scintillation counter and disintegrations per minute (DPM) was determined. The DPM was used to approximate the curies per minute emitted.

Table 2-2
Oligonucleotides used for Steady-State Kinetic Assay Substrates.

Substrate Oligonucleotides (PAGE purified)

dA gap template (34-mer)

5' GTACCCGGGGATCCGTACAGCGCATCAGCTGCAG 3'

dC gap template (34-mer)

5' GTACCCGGGGATCCGTACCGCGCATCAGCTGCAG 3'

dG gap template (34-mer)

5' GTACCCGGGGATCCGTACGGCGCATCAGCTGCAG 3'

dT gap template (34-mer)

5' GTACCCGGGGATCCGTACTGCGCATCAGCTGCAG 3'

Upstream Oligonucleotide (15-mer)

5' CTGCAGCTGATGCGC 3'

Downstream Oligonucleotide (18-mer)

5'P GTACGGATCCCCGGGTAC 3'

All oligonucleotides were purchased from Intergrated DNA Technologies (Coralville, IA)

Substrate Preparation

Four oligonucleotide substrates were used to check the Michaelis-Menton enzymatic activity. PAGE purified oligonucleotides were purchased from Intergrated DNA Technology, Coralville, IA. The upstream oligonucleotide (Table 2-2) was first 5' radiolabeled (γ-P^{32} dATP) utilizing T4 polynucleotide kinase (PNK) in PNK buffer (50mM Tris-HCl, 10mM $MgCl_2$, and 2-mercaptoethanol). Radiolabeling reaction was performed at 37°C for 30 min followed by 75°C for 5 min to terminate the reaction. A microspin G25 column (Amersham Biosciences, Buckinghamshire, England), a size exclusion column, was employed to desalt and remove the unincorporated nucleotides from the radiolabeled samples. The 5' radiolabeled upstream oligonucleotide was then added to the downstream oligonucleotide and the template oligonucleotide in a 1:2 ratio (radiolabel to nonradiolabel). Annealing took place by reducing the temperature using an Applied Biosystems 2700 thermocycler; 99°C for 5 min, 80°C for 5 min, 70°C for 5 min, 60°C for 10 min, 58°C for 10 min, 56°C for 10 min, 54°C for 10 min, 52°C for 10 min, 50°C for 10 min, 45°C for 5 min, 35°C for 5 min, and 25°C. The substrate was then dried in a vacuum centrifuge and dry substrate was stored at -20°C for up to three days before use.

Michaelis-Menton enzymatic activity assay

Activity assays were carried out for both correct and incorrect insertion of a free nucleotide into a radiolabeled single-nucleotide gapped dsDNA substrate. Reactions were performed at 15°C in 25μL containing 50mM Tris-HCl pH 8.0, 10mM $MgCl_2$, 20mM NaCl, 1mM DTT, 200μg/mL BSA, 2.5% glycerol, 0.4μM γ-P^{32}-labeled single-

nucleotide gapped DNA substrate, and the dNTP concentration ranging from 0 to 4000uM, depending upon the correct or incorrect insertion. Correct insertion reaction series were carried out through twelve separate reactions each possessing a different concentration of nucleotides (0μM, 0.0391μM, 0.0781μM, 0.1563μM, 0.3125μM, 0.625μM, 1.25μM, 2.5μM, 5μM, 10μM, 20μM, and 40μM). Incorrect dNTP insertion reactions also used twelve reactions possessing different concentrations of nucleotides (0μM, 3.91μM, 7.81μM, 15.63μM, 31.25μM, 62.5μM, 125μM, 250μM, 500μM, 1000μM, 2000μM, and 4000μM). Reactions were started with the addition of 15fmol of enzyme and were allowed to incubate for 10 min. The reactions were quenched by the addition of EDTA. Three μL samples were added to 7μL of formamide loading dye (10 mL formamide, 0.2g xylene cyanol, 0.15g bromophenol blue) and the DNA denatured at 85°C for 5 min. The products of the reaction were then separated on a 20% PAGE gel containing 7M urea for 3 to 6 hours. The DNA products were visualized in the gel by an overnight exposure of super-resolution phosphorimager screens (Packard, Meriden, CT). Screens were developed using a Packard Cyclone phosphorimager. The imager produced computer generated images that were then analyzed by selecting areas to be quantified for digital light unit (dlu) intensity. Packard Cyclone software determined the pixel intensities to derive the dlu count for each area selected. A substrate to product ratio was determined using the dlu counts from reaction products divided by the total dlu found within the lane and was correlated to the total amount of pmol of substrate contained in the initial reaction. Enzymatic velocity was determined from this value.

CHAPTER 3

RESULTS

Site Directed Mutagenesis

A cDNA representing the *X*POLβ open reading frame (ORF) was cloned from mRNA derived from *Xiphophorus maculatus* brain tissue [23]. The plasmid p*Xiph*Polβ contains the *X*POLβ ORF [23]. Site directed mutagenesis of the p*Xiph*Polβ plasmid targeted the existing nucleotide sequence of GAT, 187 nucleotides from the start codon within the *X*POLβ ORF. Site-directed mutagenesis was used to change the GAT nucleotide sequence into the nucleotide sequence CCG (Figure 3-1). A plasmid carrying this mutation p*X*polβD63P was isolated from the bacterial culture. Di-deoxynucleotide sequencing of the entire insert of p*X*polβD63P confirmed the site-directed mutation event (Figure 3-1).

Expression and purification of recombinant *X*polβ and *X*polβD63P

The pET expression system was selected due to its tight regulation of basal protein expression while utilizing an inducible promoter. The pET expression vector contains coding sequence for a translated 3 kDa N-terminal tag that facilitates purification and recognition. Site-directed mutation of p*Xiph*Polβ harboring the wild-type *Xiphophorus* POLβ ORF produced p*X*polβD63P. The dideoxynucleotide

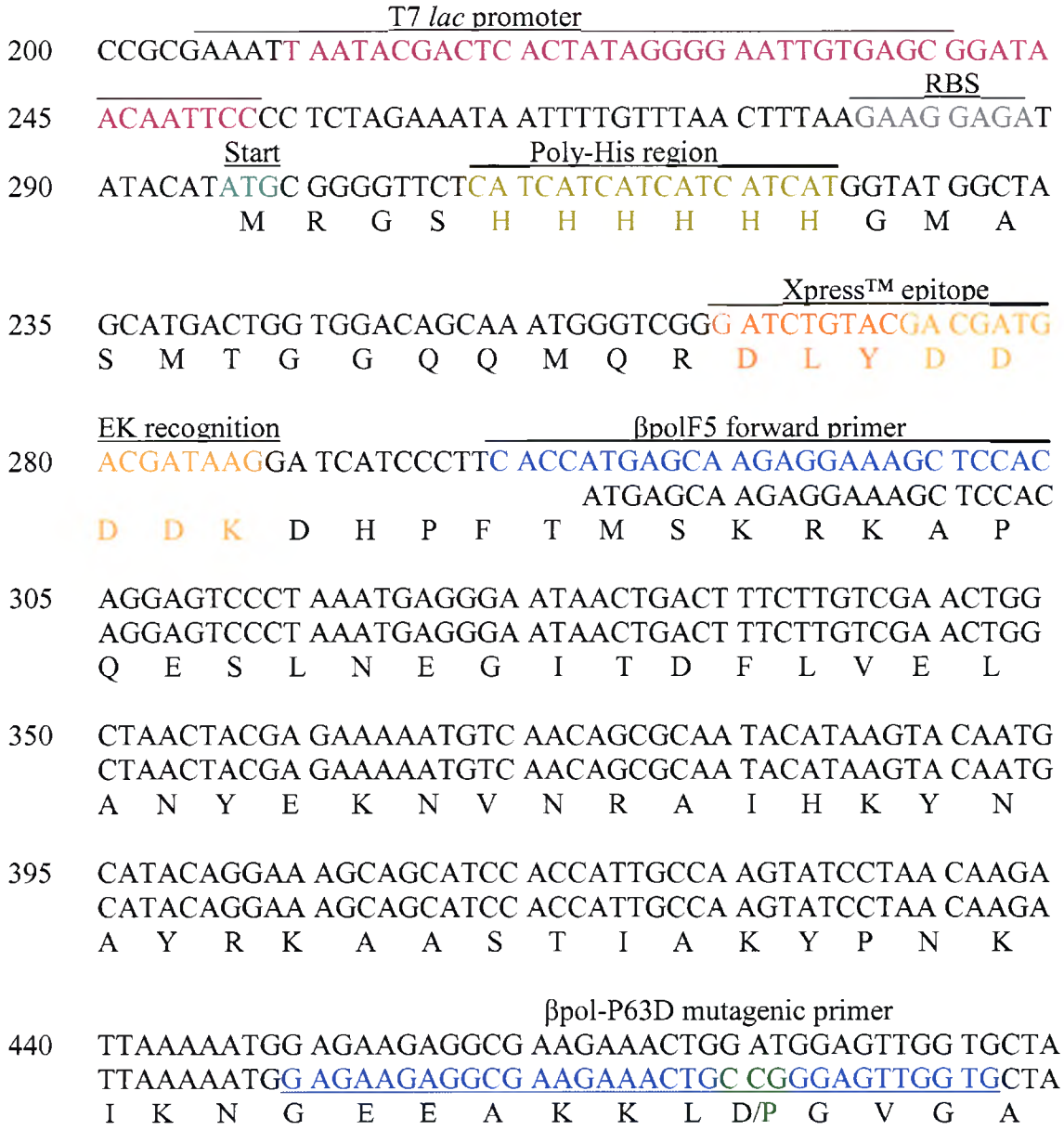

Figure 3-1 - Expression Plasmid Sequences.

Plasmid *Xiph*Polβ (top strand) and pβpolD63P DNA sequences (bottom strand) positions 200 – 385. Sequences were determined through dideoxynucleotide sequencing of each plasmid. Translation of the nucleotide sequence was determined to the expected sequence of the pET expression vector and the *X*POLβ open reading frame (ORF) sequence [18] except for the site-directed mutation at position 479-481 in pβpolD63P. *DNA shown as sequenced by Davis Sequencing, LLC. (Davis, CA).

sequencing results of the two plasmids were aligned using Clustal alignment (MacVector 7.0) to show both the success of the site-directed mutagenesis and the orientation in relation to the pET expression vector (Figure 3-1). This confirmed that p*Xiph*Polβ vectors contained the expected 1.1 kb wild-type *X*POLβ and *X*POLβD63P cDNA ORF in proper orientation with the pET expression vector. Expression of recombinant proteins was achieved by transfecting BL21DE3 *E. coli* cells (Invitrogen, Carlsbad, CA) with the purified expression plasmids p*Xiph*Polβ and p*X*polβD63P.

A pilot expression test was used to determined optimal induction time. Maximum quantity of expressed protein was expected between 3 and 4 hours post-induction, as previously reported for wild-type *X*polβ [23]. Cell culture samples were taken at 1 and 4 hours post induction and protein content visualized by gel electrophoresis. A band was observed to increase in intensity with time at the expected 42 kDa weight as determined by the comparison to a molecular weight ladder (Figure 3-2). The relative band intensities were quantified with Kodak 1D version 3.6.1 software (Eastman Kodak, New Haven, CT, USA). The expression of the mutant *X*polβD63P enzyme was not expected to be different from the previous expression of the wild-type *X*polβ enzyme. Three to four hour induction time was confirmed by the analysis of a pilot expression as shown in Figure 3-2.

Full scale expression of the mutant *X*polβ in the pET expression system yielded an average of 500μg of total protein after metal-ion chromatography purification. An SDS-PAGE gel containing the collected purification products revealed the presence of a 42kDa protein band corresponding to the expected size of the *X*polβ fusion protein (Figure 3-3). In Figure 3-3, lanes 2 and 7 contain crude cell lysate. Samples loaded in

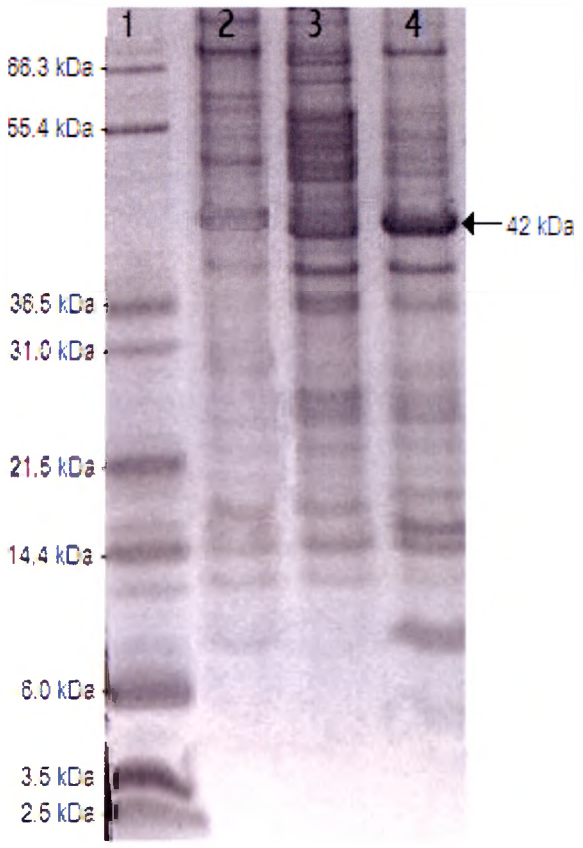

Figure 3-2 - *X*polβD63P Pilot Expression.

Pilot expression of the fusion protein *X*polβD63P was performed with SDS-PAGE in a 4-12% Bis-Tris polyacrylamide gel (Invitrogen). The gel shows an increase of a 42kDa protein after a 4 hour incubation period with the inducer IPTG. Lane 1 shows Mark12™ protein standard ladder (Invitrogen). Lane 2 shows basal level expression of the cell clone harboring *X*polβD63P prior to induction by IPTG. Lane 3 displays the appearance of a distinct band one hour after induction by IPTG. Lane 4 displays an increase in band intensity in cells four hours after IPTG induction.

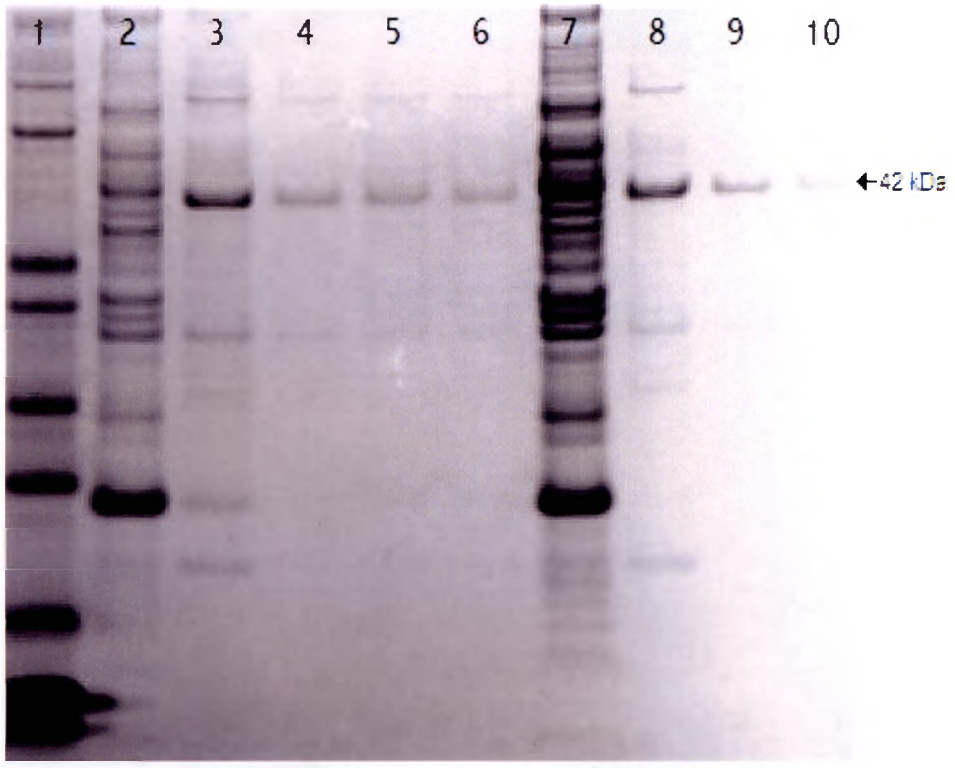

Figure 3-3 - *X*polβ Purification.

The *X*polβ and *X*polβD63P fusion proteins, after purification using a Ni^{2+} affinity chromatography column, and electrophoresis on a 4-12% Bis-Tris gel stained with Coomassie blue. Lane 1 contains Mark12™ protein ladder (Invitrogen, Carlsbad, CA). Lane 2 (*X*polβD63P) and 7 (*X*polβ) crude cell lysates from IPTG-induced cell samples. Lanes 3, 4, 5, and 6 contain samples of the eluted 1mL fractions of fusion *X*polβD63P after Ni^{2+} affinity chromatography. Lane 8, 9, and 10 contain samples of the eluted 1mL fractions of fusion *X*polβ after Ni^{2+} affinity chromatography. The arrow shows a 42kDa protein band that appears to be selected for by Ni^{2+} affinity chromatography.

lanes 3-6 contain *X*polβD63P and lanes 8-10 contain wild-type *X*polβ that have been purified by metal-ion chromatography. A band was found in the purified sample at 42kDa that was estimated to be 65% of the total protein as determined by band densities (via the Kodak 1D version 3.6.1 image analysis software). The lack of other proteins visualized by the Coomassie stain after purification through the Ni^{2+}affinity column (see lanes 3-6 and 8-10; Figure 3-3) further confirms the presence of the *X*polβ protein and the mutant *X*polβD63P.

Visualization of a protein band by Western blot using anti-Xpress antibody confirmed the presence of the anti-Xpress epitope in the Ni^{2+} eluted protein band at 42 kDa (Figure 3-4). The 42 kDa protein band was observed via comparison to the Western protein standard ladder. Some overloading of protein in Lane 2 of Figure 3-4 containing the wild-type *X*polβ sample resulted in the appearance of a slightly shifted gel band. Reactivity of *X*polβ to the mouse anti-Polβ antibody confirmed the identity of this fusion protein as *X*polβ. The dual recognition of the two antibodies (anti-Xpress and anti-Polβ) that have low cross-reactivity with other proteins coupled with the purification of protein by the metal-ion affinity chromatography confirm the isolated proteins as *X*polβ and the mutant *X*polβD63P (Figure 3-3 and 3-4).

Fusion proteins *X*polβ and *X*polβP63D were digested with enterokinase to remove the vector encoded N-terminal tag. The expected loss of 3 kDa of molecular weight was observed after enterokinase digestion (Figure 3-5). The result of the enterokinase digestion of *X*polβ and *X*polβP63D was cleavage 5 amino acids upstream from the native start methionine. Both proteins were reduced in molecular weight and a lack of other protease digestion products indicated success of the reaction without protein damage.

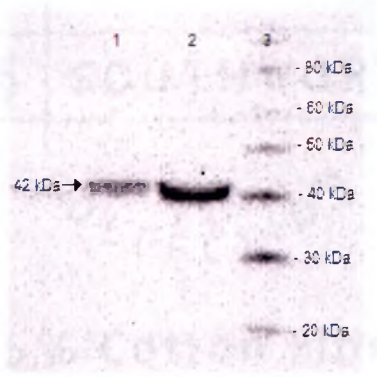

Figure 3-4 - *X*polβ Western Blot.

Detection of the *X*polβ fusion proteins observed by performing a Western Blot (Material and Methods). Fusion proteins at 42kDa (lane 1 and 2) were visualized using anti-Xpress™ antibody (Invitrogen, Carlsbad, CA) using Kodak imaging software. The anti-express antibody is specific for the expression vector encoded epitope tag. Lane 3 displays the Magik Mark™ Western protein standard (Invitrogen, Carlsbad, CA). The fusion *X*polβD63P shown in lane 1 and the fusion *X*polβ in lane 2.

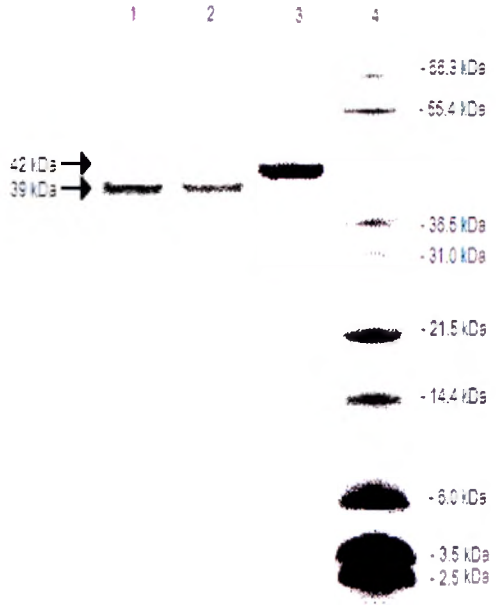

Figure 3-5 - *X*polβ Enterokinase Digestion.

Enterokinase digestion of fusion *X*polβ and fusion *X*polβD63P is captured after SDS-PAGE. The gel displays a 3kDa loss in the molecular weight in the post-EK digestion samples (lane 1 and 2). Lane 1 displays the cleaved recombinant, wild-type *X*polβ and lane 2 displays recombinant *X*polβD63P migrating at 39kDa based on the Mark 12 protein molecular ladder in lane 4. Lane 3 displays the undigested 42kDa fusion protein *X*polβ containing the N-terminal tag.

Recombinant *X*polβ P63D kinetic analyses

The specific activities of the Xpolβ and XpolβP63D enzymes were assessed by quantification of α-^{32}P dTTP that was incorporated into a dA-gapped template (Figure 3-14B, dTTP α-^{32}P labeled). The amount of radiation in each sample was determined with a scintillation counter that provided disintegrations per minute (dpm). The amount of α-^{32}P radiolabeled nucleotide incorporated per minute was derived from these data by relating the dpm counts to curie per mmol of the free radio labeled nucleotide as supplied by the manufacturer (Perkin-Elmer, Boston, MA). Specific activity of Polβ is defined as the ability to incorporate 1 nmol of α-^{32}PdTTP into a dA-gapped template per hour per mg of protein. Our *X*polβ specific activity was determined to be 3.6 x 10^4 units/mg of protein, while *X*polβD63P specific activity was determined to be 1.1 x 10^4 units/mg of protein. Previous studies of frog Polβ reported specific activities of 9 x 10^5 units/mg of protein, while chicken embryo Polβ reported 2 x 10^5 units/mg of protein and mammalian reported 4 x 10^5 – 10^6 units/mg of protein [respectively 25, 26, and 27].

Steady state kinetic reactions of *X*polβ and *X*polβD63P were performed to determine the maximum velocity and to capture the Michaelis-Menton constant (K_m) for these two recombinant proteins, while also determining the catalytic constant (K_{cat}). Products of incorporation assays were electrophoresed on 20% polyacrylamide gels and visualized using a phosphorimager (Figures 3-6A, 3-8A, 3-10A, 3-12A, 3-14A, 3-16A, 3-18A, and 3-20A). The reactions yielded a 16-mer nucleotide product representing insertion of nucleotide substrate into a single-nucleotide-gapped template (Figures 3-6B, 3-8B, 3-10B, 3-12B, 3-14B, 3-16B, 3-18B and 3-20B). Incorporation ratios were determined as a percentage of 16-mer product formed per the total 15-mer template and

16-mer product. This ratio was then related to the total amount of DNA in the reaction to obtain a velocity value for each reaction. The reciprocal velocities were then plotted against reciprocal substrate (free nucleotide) concentration in Lineweaver-Burke format (Figures 3-7, 3-9, 3-11, 3-13, and 3-15; Lineweaver-Burke Panel B). The K_{cat} and K_m were extrapolated from the Lineweaver-Burke plots and are displayed in Table 3-1. All experiments using recombinant *X*polβP63D concomitantly included the wild-type *X*polβ as a control. This allowed for direct comparison of the kinetic parameters between wild-type and mutant proteins. The catalytic efficiencies (K_{cat}/K_m) of the proteins were determined to consider both the rate of reaction and turnover of the enzyme. The steady state catalytic efficiency, K_{cat}/K_m, has been shown to be an equivalent value to the pre-steady state substrate specificity constant, K_d/K_{pol}, in both experimental data and modeling [9, 28, 29, 30]. Therefore, a ratio of the efficiency of the enzyme (error frequency and fidelity) may be calculated as shown in the equation below.

$$\text{Fidelity} = \text{Error frequency}^{-1} = ((K_{cat}/K_m)_{\text{correct}} + (K_{cat}/K_m)_{\text{incorrect}})/ (K_{cat}/K_m)_{\text{incorrect}} \quad (23)$$

dGTP incorporation into dC-gapped template

Incorporation of dGTP into a dC-gapped template is shown in Figure 3-6A. Twelve reactions with varying amounts of dGTP were individually assessed to determine the kinetic constants for each enzyme. Although the gel in Figure 3-6A shows more band dispersion than other gels; the bands are easily distinguished both between lanes and in the individual lanes. This added dispersion could have resulted from the longer run time or incomplete deionization of the gel matrix. Areas of the gel were selected to include gel bands, while paying careful attention to maintain the same size areas when comparing two bands in the same lane. The Packard Cyclone phosphorimager determined dlu count

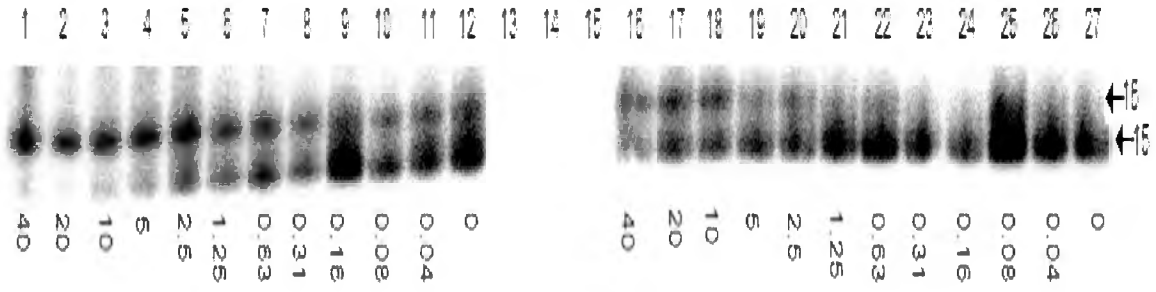

A. μM μM

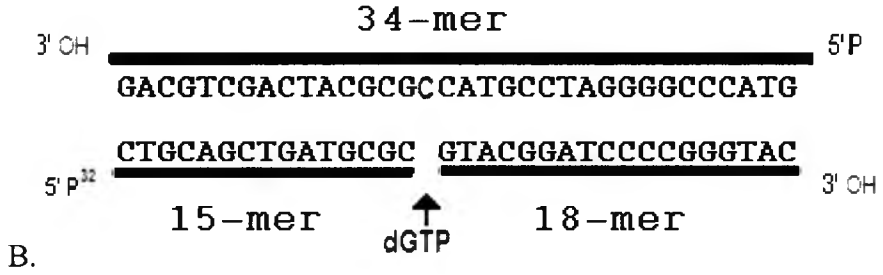

B.

Figure 3-6 - dC gap – dGTP Incorporation Assay Gel Image.

Sixteen-mer and 15-mer reaction product from the reaction were fractionated on PAGE at 800Vh. The *X*polβD63P samples were loaded in lanes 1-12 while control *X*polβ samples are in lanes 16-27. The reaction series employed a dGTP concentration of 0-40μM. Phosphorimager screens were exposed overnight to the gels containing the separated radioactive oligonucleotides. The gel image was produced using Packard cyclone phosphorimager software from data collected from the phosphorimager screens. Regions of this gel image were blocked off in identical sizes for products and templates to assess dlu counts.

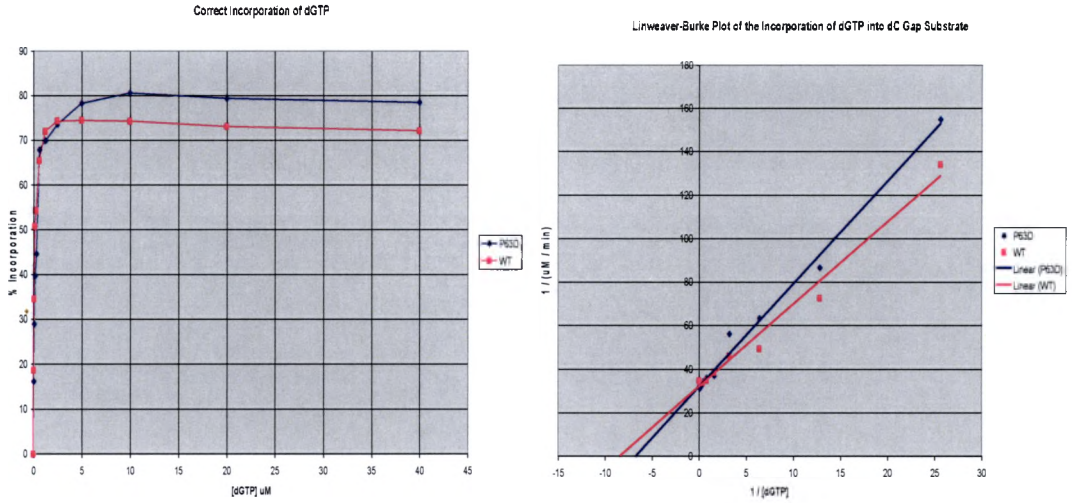

Panel A Panel B

Figure 3-7 - dC gap – dGTP Incorporation Assay Plots.

Panel A: Dlu counts were collected from the gel images by the Packard Optiquant software. Amounts of both the 16-mer reaction product and the 15-mer reaction template were obtained and compared to calculate the % incorporation of dGTP (16-mer product: 16-mer + 15-mer template). Michaelis-Menton plot shows the % incorporation per the concentration of dGTP. The percent of incorporation was multiplied by the total amount of substrate contained within the reaction to determine the reaction velocity. Panel B: A Lineweaver-Burke plot shows the inverse of the reaction velocities per the inverse dGTP concentration. The K_m and V_{max} values (See Figure 3-1) are obtained from the y- and x-intercepts of the Lineweaver-Burke plots.

for each of the selected areas. The data analyses are presented in Figure 3-7 for a single reaction series for both enzymes from a single PAGE experiment. Panel A shows up to 80% of the template incorporated free dGTP nucleotide when the *X*polβD63P enzyme was used, while the wild-type *X*polβ protein added free dGTP nucleotide into up to 75% of the template. Panel B shows a Lineweaver-Burke plot. The average K_m for *X*polβD63P was 0.97μM and the average K_m for wild-type was 0.41μM. The increase in the K_m of the mutant enzyme suggests that the enzyme's affinity for the substrate may be increased, however the deviation neglects any observed difference. The average K_{cat}/K_m for *X*polβD63P was $1.3\mu M^{-1}s^{-1}$ and for wild-type *X*polβ was $2.1\mu M^{-1}s^{-1}$. The Lineweaver-Burke plot shows the two plots to intersect at the y-intercepts. Intersection of the y-intercepts suggests a similar V_{max}.

dTTP incorporation into dA-gapped template

Incorporation of dTTP into a dA-gapped template is shown in Figure 3-14. Twelve reactions with varying amounts of dTTP (0-40μM) were individually assessed to determine the kinetic constants for each enzyme. Although the gel in Figure 3-14 shows more band dispersion than other gels; the bands are easily distinguished both between lanes and in the individual lanes. Areas of the gel were selected for computer analyses include gel bands and maintain the same area for comparison of two bands in the same lane. The Packard Cyclone phosphorimager produced dlu counts for each of the selected gel areas. Data was collected and presented in Figure 3-15 for a single reaction series of each enzyme from a single PAGE experiment. Panel A shows up to 74% of the template has been incorporated with the free dGTP nucleotide when the *X*polβD63P was used,

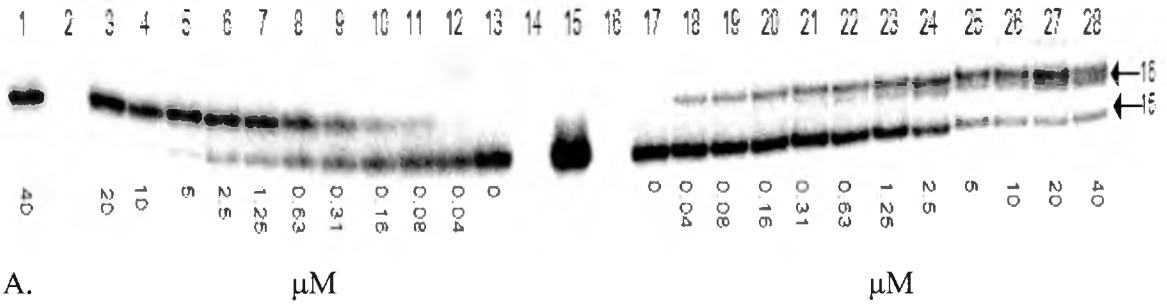

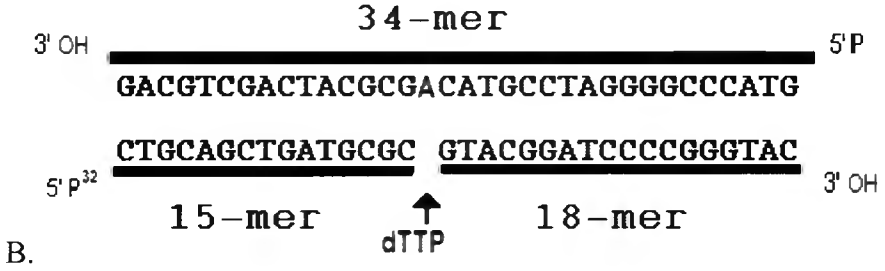

Figure 3-8 - dA gap – dTTP Incorporation Assay Gel Image.

Samples were fractionated using a 20% denaturing PAGE for 600Vh. Phosphorimager produced gel image derived from overnight exposure of phosphorimager screens. The gel image shows *X*polβD63P reaction products on the left while control, *X*polβ, reaction products are on the right. An oligonucleotide ladder and blank lanes were used for gel orientation (lanes 2, 15, 14, and 16). The gel image produced by the Packard phosphorimager system shows the reaction series across the concentration gradient of dTTP (0-40μM). The *X*polβD63P are in lanes 1 and 3-13 while controls, Xpolβ, are in lanes 17-28. Lane 15 is a radiolabeled oligonucleotide ladder (bottom to top; 15-mer and 16-mer).

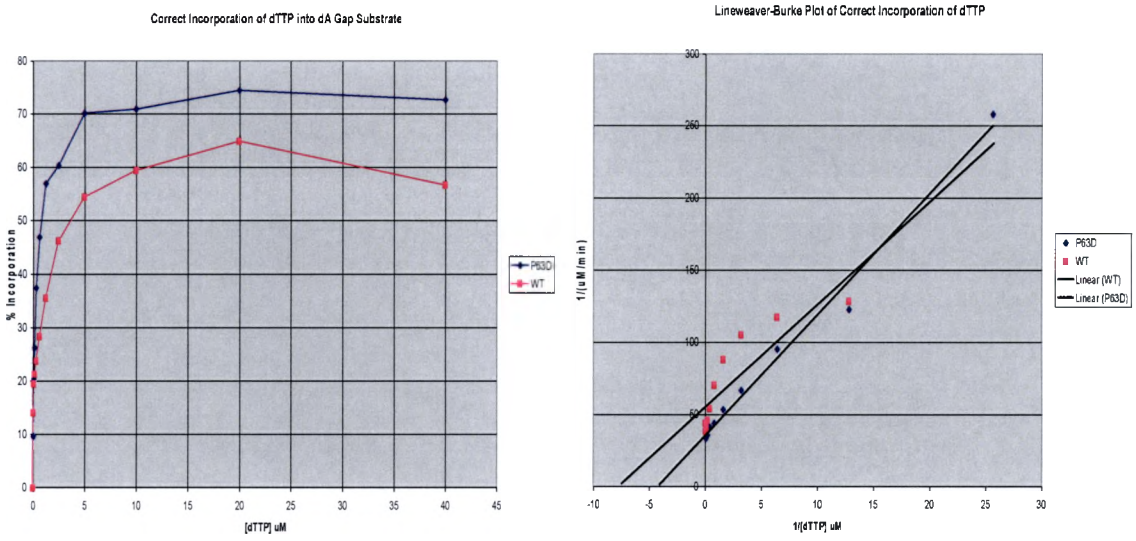

Panel A Panel B

Figure 3-9 - dA gap – dTTP Incorporation Assay Plots.

Panel A: Data from the reaction gel images (Figure 3-14) analyzed by Packard Optiquant software. The ratio of two observed bands (16-mer product: 16-mer + 15-mer template) yielded the % dTTP incorporation into the substrate. The % substrate incorporation is plotted in Panel A versus the concentration of dTTP (μM). The % incorporation is multiplied by the picomoles of substrate in each reaction to derive a reaction velocity for each lane. Panel B: A Lineweaver-Burke plot was plotted using the inverse velocity of each reaction versus the inverse dTTP concentrations. The K_m and V_{max} values (See Figure 3-1) are obtained from y- and x-intercepts of the Lineweaver-Burke plot.

while the wild-type *X*polβ incorporated the free dGTP nucleotide into up to 66% of the template. Panel B shows a Lineweaver-Burke plot. The average K_m for *X*polβD63P was 1.21 μM and the average K_m for wild-type was 0.75 μM. The increase in the K_m of the mutant enzyme suggests that the enzyme's affinity for the substrate has increased. The average K_{cat}/K_m for *X*polβD63P was 1.6 $\mu M^{-1}*s^{-1}$ and the average K_{cat}/K_m for wild-type *X*polβ was 1.4 $\mu M^{-1}*s^{-1}$. The Lineweaver-Burke plot depicts the two plots to intersect at the y-intercepts suggesting that the V_{max} may be similar.

dATP incorporation into dT-gapped template

Incorporation of dATP into a dT-gapped template is shown in Figure 3-8. The reaction series for each enzyme included 12 individual dATP concentrations to test concentration points between 0 to 40μM dATP. The last point in the series is a blank containing no dATP to react with the substrate and enzyme. This gel showed distinguishable band separation for data acquisition. A blank lane (Lane 2, Figure 3-8A) was used to determine gel orientation. Figure 3-8A, lane 9 and 24 displays the result of small bubbles in the gel sample lane; however data was able to be collected from these two gel lanes. Figure 3-8A, lane 6 depicts a troubling problem of a reaction that is inconsistent with the reaction gradient pattern of the other reactions. This is observed infrequently. Areas of the gel selected for computer analyses encompass gel bands and maintained the same area for comparison of two bands in the same lane. The Packard Cyclone phosphorimager produced dlu counts for each of the selected gel areas. Data were collected and are presented in Figure 3-9. Figure 3-9, panel A shows *X*polβD63P incorporated free dATP nucleotide into up to 75% of the template while the wild-type

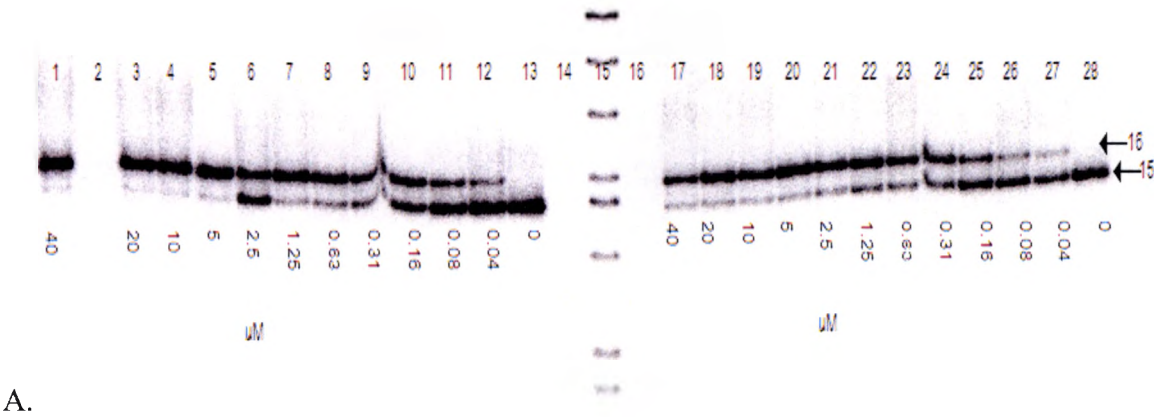

A.

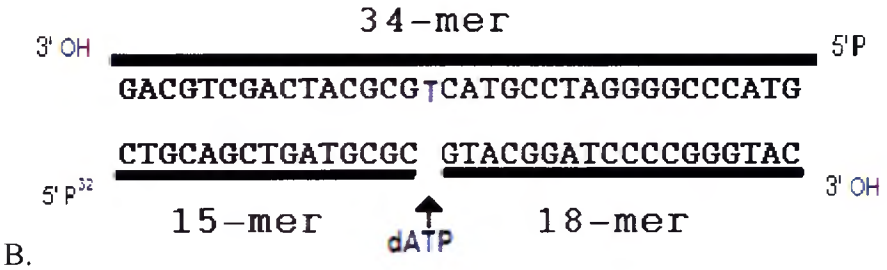

B.

Figure 3-10 - dT gap – dATP Incorporation Assay Gel Image.

Samples were fractionated using a 20% denaturing PAGE for 600Vh. Phosphorimager produced gel image derived from overnight exposure of phosphorimager screens. The gel image shows *X*polβD63P reaction products on the left while control, *X*polβ, reaction products are on the right. An oligonucleotide ladder and blank lanes were used for gel orientation (lanes 2, 15, 14, and 16). Regions of this gel image were blocked off in identical sizes for products and substrates to assess dlu counts. Lanes 1 and 3-13 are *X*polβD63P reaction series (0-40μM of dATP). Lane 17-28 are *X*polβ reaction series (0-40μM of dATP). Lane 15 is a radiolabeled oligonucleotide ladder (bottom to top; 8-mer, 9-mer, 12-mer, 15-mer, 16-mer, 18-mer, 22-mer, and 24-mer).

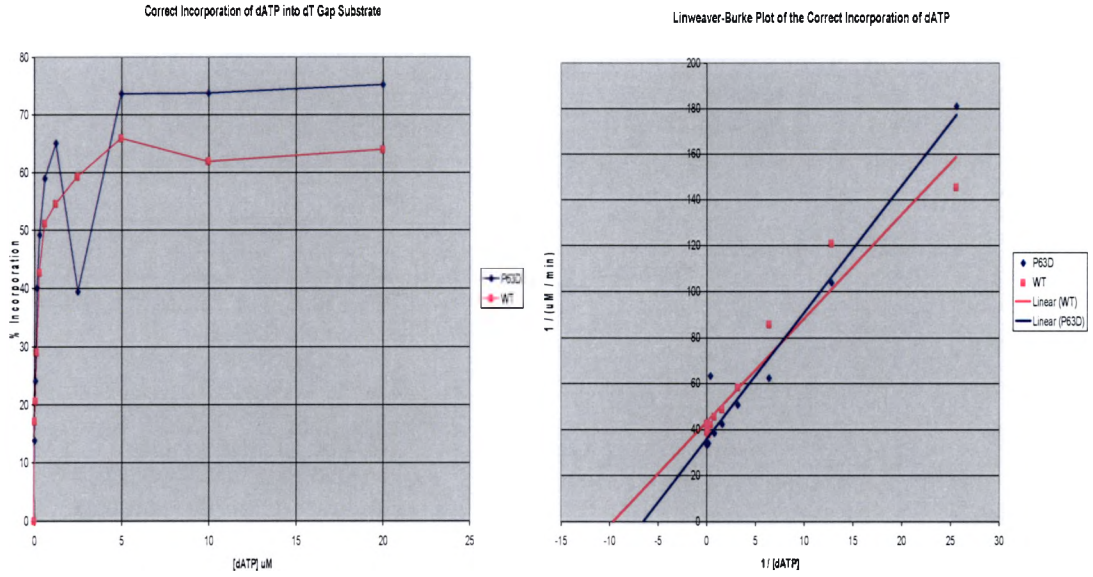

Panel A Panel B

Figure 3-11 - dT gap – dATP Incorporation Assay Plots.

Panel A: Data from the reaction gel images (Figure 3-8) analyzed by Packard Optiquant software. The ratio of two observed bands (16-mer product: 16-mer + 15-mer template) yielded the % dATP incorporation into the substrate. The % substrate incorporation is plotted in Panel A versus the concentration of dATP (μM). The % incorporation is multiplied by the picomoles of substrate in each reaction to derive a reaction velocity for each lane. Panel B: A Lineweaver-Burke plot was plotted using the inverse velocity of each reaction versus the inverse dATP concentrations. The K_m and V_{max} values (See Figure 3-1) are obtained from y- and x-intercepts of the Lineweaver-Burke plot.

*X*polβ incorporated free dATP nucleotide into up to 65% of the template. All assays shown are substrate saturating. The average K_m for *X*polβD63P was 0.19μM and the average K_m for wild-type was 0.35 μM. The average K_{cat}/K_m for *X*polβD63P was 4.1$\mu M^{-1}s^{-1}$ and the average K_{cat}/K_m for wild-type *X*polβ was 3.5$\mu M^{-1}s^{-1}$.

dCTP incorporation into dT-gapped template

Incorporation of dCTP into a dT gapped template is shown in Figure 3-10A. Twelve reactions with varying amounts of dCTP (0-4000μM) were individually assessed to determine the steady-state kinetic constants for each enzyme. The gel was run for 600 Vhrs and produced ample separation with minimal band dispersion. Areas of the gel selected for computer analyses encompass gel bands and maintained the same area for comparison of two bands in the same lane. The Packard Cyclone phosphorimager produced dlu counts for each of the selected gel areas. The analyses of the dlu counts from the phosphorimage of the gel allowed for graphs contained in Figure 3-11.

Data presented in the graphs of Figure 3-11 represent both enzymes' individual twelve enzymatic reactions plotted from a single PAGE experiment. Panel A shows the wild-type incorporated the free dCTP into up to 70% of the template. The *X*polβD63P incorporated the free dCTP nucleotide into up to 58% of the template. The average K_m for *X*polβD63P was 22.8 μM and the average K_m for wild-type was 54.2μM. The average K_{cat}/K_m for *X*polβD63P was 0.028 $\mu M^{-1}s^{-1}$ and the average K_{cat}/K_m for wild-type *X*polβ was 0.038 $\mu M^{-1}s^{-1}$. The Lineweaver-Burke plot depicts the two plots running parallel. Parallel lines on the Lineweaver Burke plot indicate that both the V_{max} and K_m are differing. The catalytic efficiency was observed as unaffected by the results.

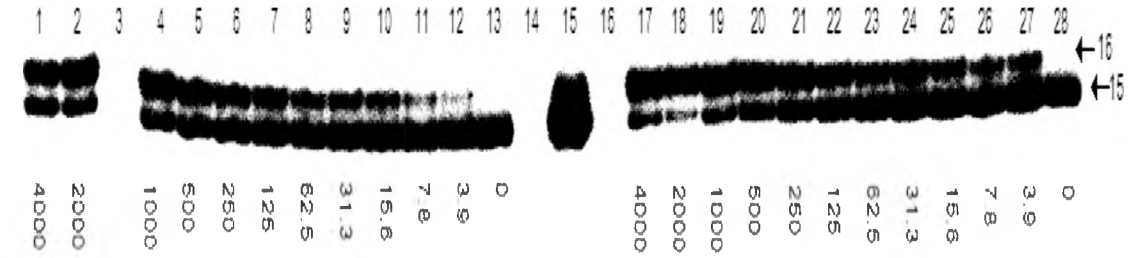

A. μM μM

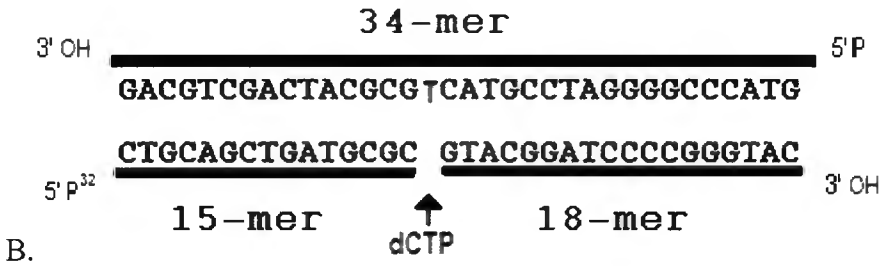

B.

Figure 3-12 - dT gap – dCTP Incorporation Assay Gel Image.

Samples were fractionated using a 20% denaturing PAGE for 600Vh. Phosphorimager produced gel image derived from overnight exposure of phosphorimager screens. The gel image shows *X*polβD63P reaction products on the left while control, *X*polβ, reaction products are on the right. An oligonucleotide ladder and blank lanes were used for gel orientation (lanes 3, 14, 15, and 16). The gel image produced by the Packard phosphorimager system shows the reaction series across the concentration gradient of dCTP (0-4000μM). The *X*polβD63P products are in lanes 1, 2, and 4-13 while controls, from *X*polβ, are in lanes 17-28. Lane 15 is a radiolabeled oligonucleotide ladder (bottom to top; 15-mer and 16-mer). Regions of this gel image were blocked off in identical sizes for products and substrates to assess dlu counts.

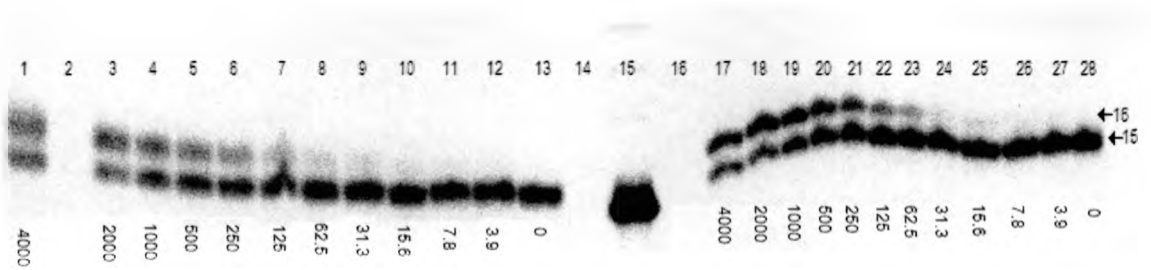

A. μM μM

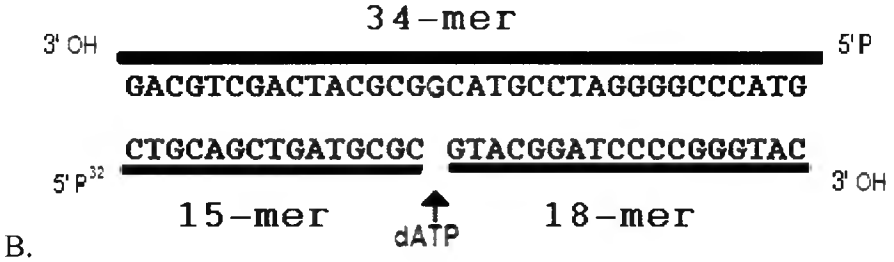

B.

Figure 3-18 - dG gap – dATP Incorporation Assay Gel Image.

Samples were fractionated using a 20% denaturing PAGE for 600Vh. Phosphorimager produced gel image derived from overnight exposure of phosphorimager screens. The gel image shows *X*polβD63P reaction products on the left while control, *X*polβ, reaction products are on the right. An oligonucleotide ladder and blank lanes were used for gel orientation (lanes 2, 15, 14, and 16). The gel image produced by the Packard phosphorimager system shows the reaction series across the concentration gradient of dATP (0-4000μM). The *X*polβD63P are in lanes 1 and 3-13 while controls, Xpolβ, are in lanes 17-28. Lane 15 is a radiolabeled oligonucleotide ladder (bottom to top; 8-mer, 9-mer, 12-mer, 15-mer, 16-mer, 18-mer, 22-mer, and 24-mer).

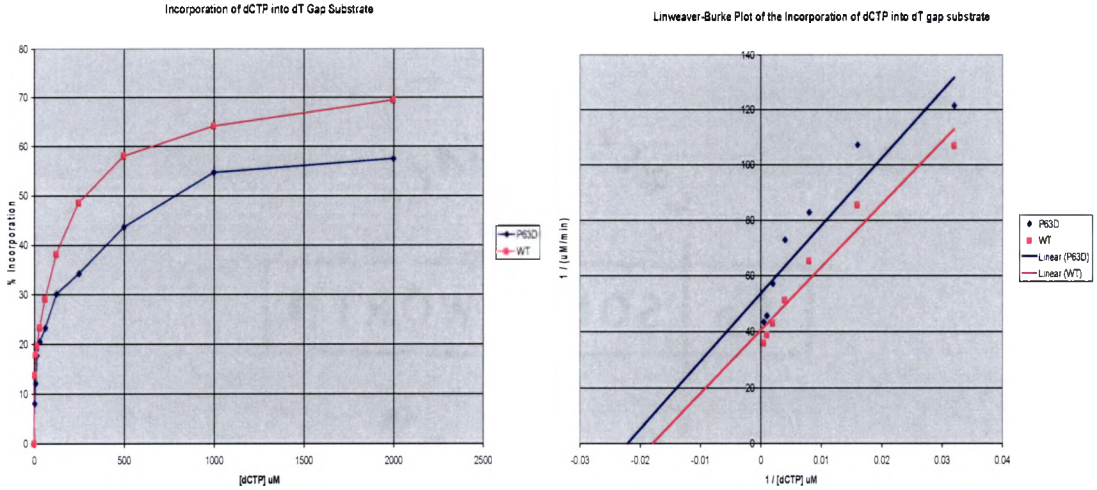

Panel A Panel B

Figure 3-13 - dT gap – dCTP Incorporation Assay Plots.

Panel A: Data from the reaction gel images (Figure 3-8) analyzed by Packard Optiquant software. The ratio of two observed bands (16-mer product: 16-mer + 15-mer template) yielded the % dCTP incorporation into the substrate. The % substrate incorporation is plotted in Panel A versus the concentration of dCTP (μM). The % incorporation is multiplied by the picomoles of substrate in each reaction to derive a reaction velocity for each lane. Panel B: A Lineweaver-Burke plot was plotted using the inverse velocity of each reaction versus the inverse dCTP concentrations. The K_m and V_{max} values (See Figure 3-1) are obtained from y- and x-intercepts of the Lineweaver-Burke plot.

dGTP incorporation into dT-gapped template

Incorporation of dGTP into a dT-gapped template is shown in Figure 3-12. Twelve reactions with varying amounts of dGTP (0-4000μM) were individually assessed to determine the kinetic constants for each enzyme. Figure 3-12A, lane 7 displays the results of small bubbles in the gel lane. Band separation allowed for both data sets to be collected. Areas of the gel selected for computer analyses encompass gel bands and maintained the same area for comparison of two bands in the same lane. The Packard Cyclone phosphorimager produced dlu counts for each of the selected gel areas. The data analysis is presented in Figure 3-13 for a single reaction series of each enzyme. Panel A shows up to 68% of the template has been incorporated with the free dGTP nucleotide when the *X*polβD63P was used, while the wild-type *X*polβ incorporated the free dGTP nucleotide into up to 53% of the template. Panel B presents a Lineweaver-Burke plot. The average K_m for *X*polβD63P was 13.3μM and the average K_m for wild-type was 6.2μM. The average K_{cat}/K_m for *X*polβD63P was $0.053\mu M^{-1}s^{-1}$ and the average K_{cat}/K_m for wild-type *X*polβ was $0.067\mu M^{-1}s^{-1}$.

dCTP incorporation into dG-gapped template

Incorporation of dCTP into a dG-gapped template is shown in Figure 3-16. Twelve reactions with varying amounts of dCTP (0-40μM) were individually assessed to determine the kinetic constants for each enzyme. Lanes in the gel matrix of Figure 3-16 show a great deal of dispersion due to an increase of Vh. This gel shows distinguishable band separation for data acquisition. Areas of the gel selected for computer analyses included gel bands and maintained the same area for comparison of two bands in the

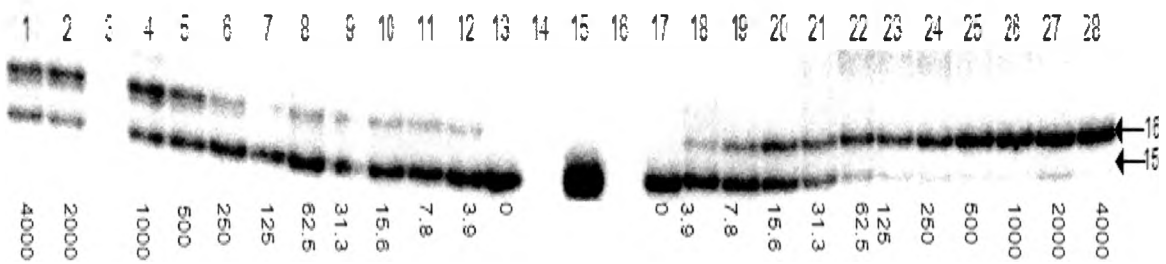

A. μM μM

B.

Figure 3-14 - dT gap – dGTP Incorporation Assay Gel Image.

Samples were fractionated using a 20% denaturing PAGE for 600Vh. Phosphorimager produced gel image derived from overnight exposure of phosphorimager screens. The gel image shows *X*polβD63P reaction products on the left while control, *X*polβ, reaction products are on the right. An oligonucleotide ladder and blank lanes were used for gel orientation (lanes 3, 15, 14, and 16). The gel image produced by the Packard phosphorimager system shows the reaction series across the concentration gradient of dGTP (0-4000μM). The *X*polβD63P products are in lanes 1, 2, and 4-13 while controls, Xpolβ products, are in lanes 17-28.

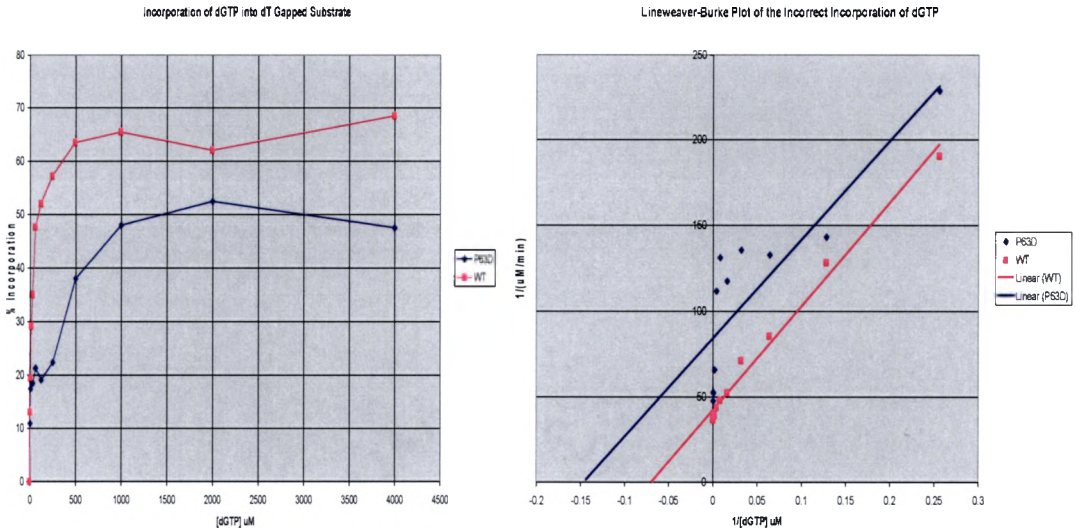

Panel A Panel B

Figure 3-15 - dT gap – dGTP Incorporation Assay Plots.

Panel A: Data from the reaction gel images (Figure 3-12) analyzed by Packard Optiquant software. The ratio of two observed bands (16-mer product: 16-mer + 15-mer template) yielded the % dGTP incorporation into the substrate. The % substrate incorporation is plotted in Panel A versus the concentration of dGTP (μM). The % incorporation is multiplied by the picomoles of substrate in each reaction to derive a reaction velocity for each lane. Panel B: A Lineweaver-Burke plot was plotted using the inverse velocity of each reaction versus the inverse dGTP concentrations. The K_m and V_{max} values (See Figure 3-1) are obtained from y- and x-intercepts of the Lineweaver-Burke plot.

same lane. The Packard Cyclone phosphorimager produced dlu counts for each of the selected gel areas. The data analyses are presented in Figure 3-17 for a single reaction series of each enzyme from a single PAGE experiment. Panel A shows up to 88% of the template has been incorporated with the free dCTP nucleotide when the *X*polβD63P was used, while the wild-type *X*polβ incorporated the free dCTP nucleotide into up to 88% of the template. Panel B shows a Lineweaver-Burke plot. The average K_m for *X*polβD63P was 0.98μM and the average K_m for wild-type was 1.44μM. The average K_{cat}/ K_m for *X*polβD63P was 0.82$\mu M^{-1}s^{-1}$ and the average K_{cat}/K_m for wild-type *X*polβ was 0.93$\mu M^{-1}s^{-1}$. The Lineweaver-Burke plot depicts the intersection of the two plots at the x-intercepts suggesting a similar K_m.

dATP incorporation into dG-gapped template

Incorporation of dATP into a dG-gapped template is shown in Figure 3-18. Twelve reactions with varying amounts of dATP (0-4000μM) were individually assessed to determine the kinetic constants for each enzyme. Lane 7 in Figure 3-18A displays the result of small bubbles present in the gel matrix. This gel shows distinguishable band separation for data acquisition. Areas of the gel selected for computer analyses included gel bands and maintained the same area for comparison of two bands in the same lane. The Packard Cyclone phosphorimager produced dlu counts for each of the selected gel areas. The data analyses are presented in Figure 3-17 for a single reaction series of each enzyme from a single PAGE experiment. Panel A shows up to 46% of the template incorporated with the free dATP nucleotide when the *X*polβD63P was used, while the wild-type *X*polβ incorporated the free dATP nucleotide into up to 57% of the template.

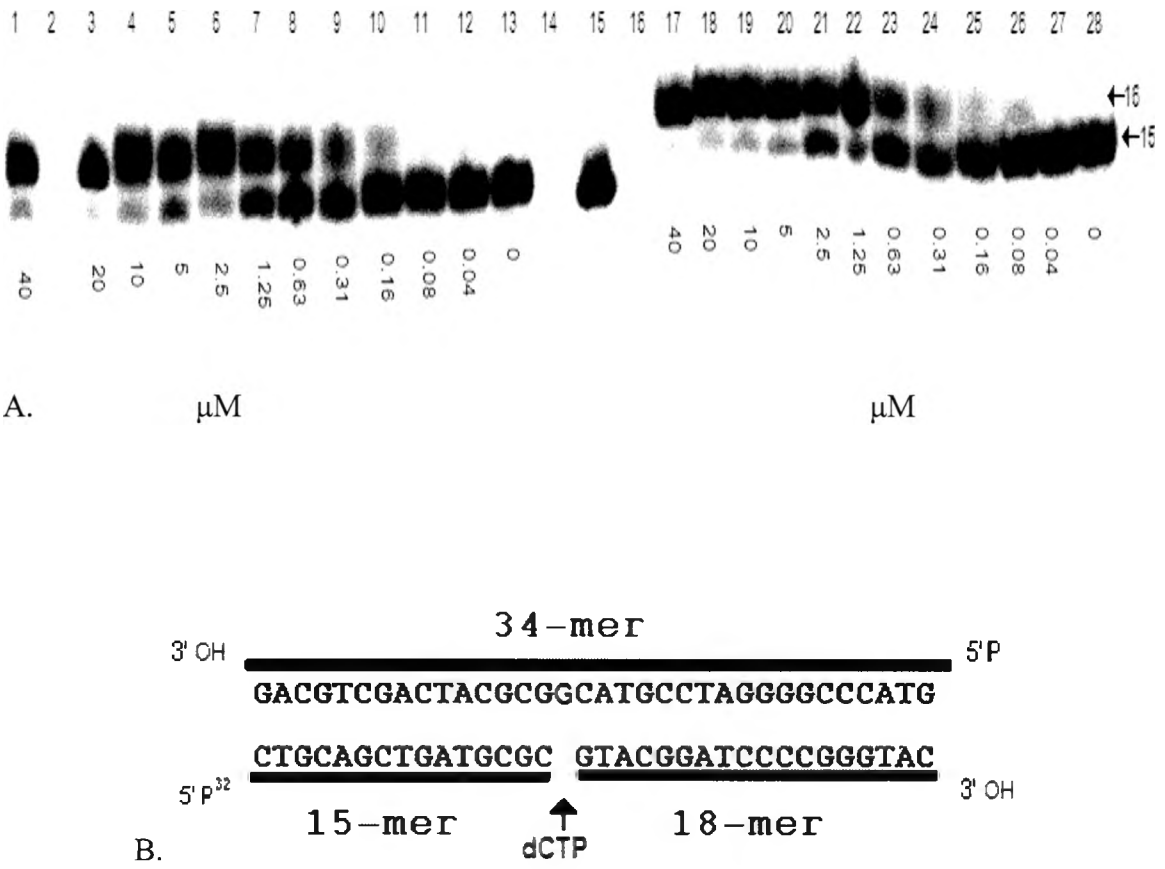

Figure 3-16 - dG gap – dCTP Incorporation Assay Gel Image.

Samples were fractionated using a 20% denaturing PAGE for 900Vh. Phosphorimager produced gel image derived from overnight exposure of phosphorimager screens. The gel image shows *X*polβD63P reaction products on the left while control, *X*polβ, reaction products are on the right. An oligonucleotide ladder and blank lanes were used for gel orientation (lanes 2, 15, 14, and 16). The gel image produced by the Packard phosphorimager system shows the reaction series across the concentration gradient of dCTP (0-40 μM). The *X*polβD63P are in lanes 1 and 3-13 while controls, Xpolβ, are in lanes 17-28.

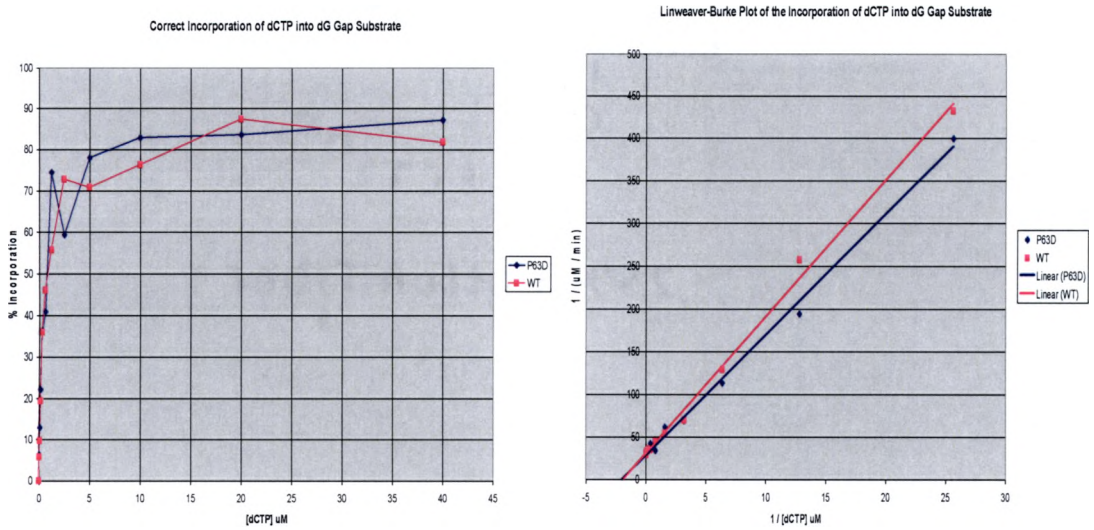

Panel A Panel B

Figure 3-17 - dG gap – dCTP Incorporation Assay Plots.

Panel A: Data from the reaction gel images (Figure 3-16) analyzed by Packard Optiquant software. The ratio of two observed bands (16-mer product: 16-mer + 15-mer template) yielded the % dCTP incorporation into the substrate. The % substrate incorporation is plotted in Panel A versus the concentration of dCTP (μM). The % incorporation is multiplied by the picomoles of substrate in each reaction to derive a reaction velocity for each lane. Panel B: A Lineweaver-Burke plot was plotted using the inverse velocity of each reaction versus the inverse dCTP concentrations. The K_m and V_{max} values (See Figure 3-1) are obtained from y- and x-intercepts of the Lineweaver-Burke plot.

Panel B shows a Lineweaver-Burke plot. The average K_m for *X*polβD63P was 103.5μM and the average K_m for wild-type was 78.6μM. The average K_{cat}/K_m for *X*polβD63P was $0.000031\mu M^{-1}s^{-1}$ and the average K_{cat}/K_m for wild-type *X*polβ was $0.000029\mu M^{-1}s^{-1}$. The Lineweaver-Burke plot depicts the intersection at the x-intercepts of the two plots suggests a similar K_m.

dTTP incorporation into dG-gapped template

Incorporation of dTTP into a dG-gapped template is shown in Figure 3-20. Twelve reactions with varying amounts of dTTP (0-4000μM) were individually assessed to determine the kinetic constants for each enzyme. This gel shows distinguishable band separation for data acquisition. Areas of the gel selected for computer analyses included gel bands and maintained the same area for comparison of two bands in the same lane. The Packard Cyclone phosphorimager produced dlu counts for each of the selected gel areas. The data analyses are presented in Figure 3-17 for a single reaction series of each enzyme from a single PAGE experiment. Panel A shows up to 54% of the template has been incorporated with the free dTTP nucleotide when the *X*polβP63D was used, while the wild-type *X*polβ incorporated the free dTTP nucleotide into up to 70% of the substrate. Panel B shows a Lineweaver-Burke plot. The average K_m for *X*polβD63P was 34.5μM and the average K_m for wild-type was 58.8μM. The average K_{cat}/K_m for *X*polβD63P was $0.0010\mu M^{-1}*s^{-1}$ and the average K_{cat}/K_m for wild-type *X*polβ was $0.0039\mu M^{-1}s^{-1}$. A three-fold increase the K_{cat}/K_m was observed. The Lineweaver-Burke plot depicts the intersection of the two plots at the x-intercept suggesting a similar K_m.

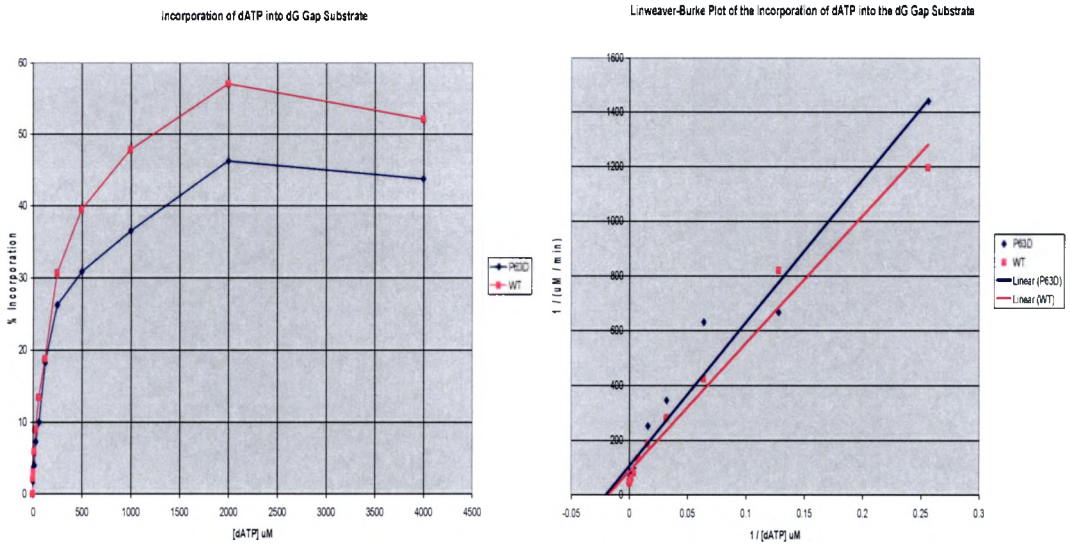

Panel A Panel B

Figure 3-19 - dG gap – dATP Incorporation Assay Plots.

Panel A: Data from the reaction gel images (Figure 3-8) analyzed by Packard Optiquant software. The ratio of two observed bands (16-mer product: 16-mer + 15-mer template) yielded the % dATP incorporation into the substrate. The % substrate incorporation is plotted in Panel A versus the concentration of dATP (μM). The % incorporation is multiplied by the picomoles of substrate in each reaction to derive a reaction velocity for each lane. Panel B: A Lineweaver-Burke plot was plotted using the inverse velocity of each reaction versus the inverse dATP concentrations. The K_m and V_{max} values (See Figure 3-1) are obtained from y- and x-intercepts of the Lineweaver-Burke plot.

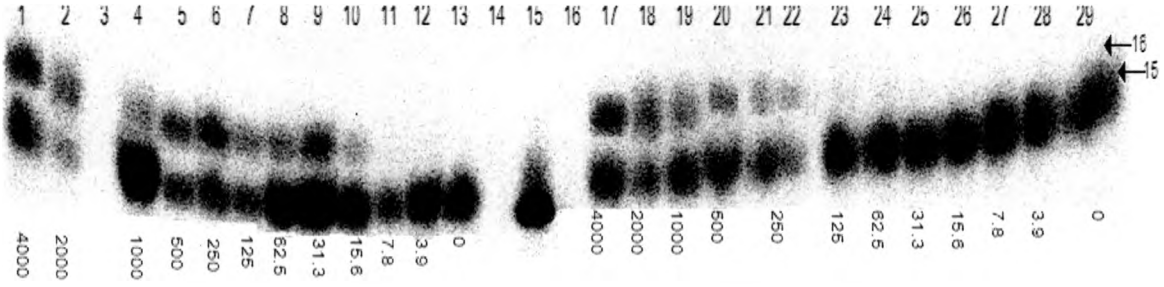

A. μM μM

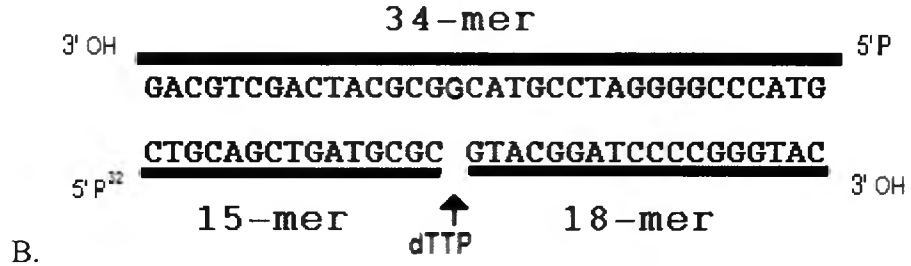

B.

Figure 3-20 - dG gap – dTTP Incorporation Assay Gel Image.

Samples were fractionated using a 20% denaturing PAGE for 700Vh. Phosphorimager produced gel image derived from overnight exposure of phosphorimager screens. The gel image shows *X*polβD63P reaction products on the left while control, *X*polβ, reaction products are on the right. An oligonucleotide ladder and blank lanes were used for gel orientation (lanes 2, 15, 14, and 16). The gel image produced by the Packard phosphorimager system shows the reaction series across the concentration gradient of dTTP (0-4000μM). The *X*polβD63P are in lanes 1, 2, and 4-13 while controls, Xpolβ, are in lanes 17-29. Lane 22 and 21 displays the results of a broken well lane prior to gel run. Contamination of lane 22 can be observed in the phosphorimage. The data collected was still considered viable because the ratio of the two values was assumed to be equally affected.

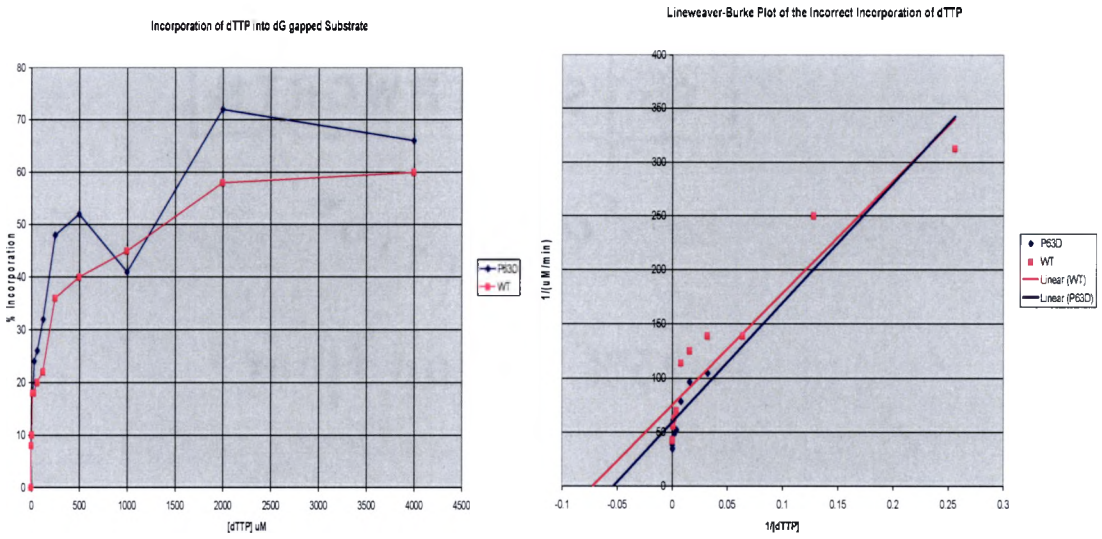

Panel A Panel B

Figure 3-21 - dG gap – dTTP Incorporation Assay Plots.

Panel A: Data from the reaction gel images (Figure 3-20) analyzed by Packard Optiquant software. The ratio of two observed bands (16-mer product: 16-mer + 15-mer template) yielded the % dTTP incorporation into the substrate. The % substrate incorporation is plotted in Panel A versus the concentration of dTTP (μM). The % incorporation is multiplied by the picomoles of substrate in each reaction to derive a reaction velocity for each lane. Panel B: A Lineweaver-Burke plot was plotted using the inverse velocity of each reaction versus the inverse dTTP concentrations. The K_m and V_{max} values (See Figure 3-1) are obtained from y- and x-intercepts of the Lineweaver-Burke plot.

Comparison of Recombinant *X*polβ and *X*polβD63P

Compiled K_m, K_{cat}/K_m, error frequencies, and fidelities are included in Table 3-1. The data shown in Table 3-1 displays the comparative analysis of mutant *X*polβD63P and wild-type *X*polβ. The fidelities and error frequencies were calculated through the equation:

$$\text{Fidelity} = \text{Error frequency}^{-1} = ((K_{cat}/K_m)_{correct} + (K_{cat}/K_m)_{incorrect})/ (K_{cat}/K_m)_{incorrect} \quad [23]$$

Fidelity was assessed to determine a ratio that may reflect the incorporation of bases that do not follow Watson-Crick base pairing rules. Fidelity and error frequency were measured for the dT-gapped and the dG-gapped templates. Fidelity for incorporation of dCTP into the dT-gapped template was calculated to be 1 in 147 and 1 in 92 for mutant *X*polβD63P and wild-type *X*polβ, respectively. Fidelity for incorporation of dGTP into the dT-gapped template was calculated to be 1 in 78 and 1 in 53 for mutant *X*polβD63P and wild-type *X*polβ, respectively. Fidelity for incorporation of dATP into the dG-gapped template was calculated to be 1 in 25,400 and 1 in 35,300 for mutant *X*polβD63P and wild-type *X*polβ, respectively. Fidelity for incorporation of dATP into the dG gapped template was calculated to be 1 in 793 and 1 in 240 for mutant *X*polβD63P and wild-type *X*polβ, respectively. Notably the incorporation of dTTP into the dG gapped template shows a three-fold increase in the mutant *X*polβD63P. The error frequencies were also calculated as the inverse of the fidelity.

Table 3-1
Michaelis-Menton Constant, Catalytic Efficiency, Fidelity, and Error Frequency Comparison of Recombinant *X*polβ and *X*polβD63P

Template-dNTP	K_m(μM)	K_{cat}/K_m($\mu M^{-1} s^{-1}$)	Fidelity	Error Frequency
dA-dTTP				
D63P	1.21 ± 0.9	1.6 ± 1.2		
WT	0.75 ± 0.3	1.4 ± 0.9		
dC-dGTP				
D63P	0 97 ± 0.4	1.3 ± .7		
WT	0.41 ± 0.2	2.1 ± .1		
dT-dATP				
D63P	0.19 ± 0 05	4 1 ± 0.07		
WT	0 35 ± 0.17	3.5 ± 1.2		
dT-dCTP				
D63P	22.8 ± 8.9	0 028 ± 0 007	147	0 007
WT	54 2 ± 40	0.038 ± 0.017	92	0.011
dT-dGTP				
D63P	13.3 ± 3.3	0.053 ± 0.007	78	0.013
WT	6.2 ± 1.1	0.067 ± 0 002	53	0 019
dG-dCTP				
D63P	0.98 ± 0.2	0.82 ± 0 5		
WT	1 44 ± 0.4	0 93 ± 0.5		
dG-dATP				
D63P	103.5 ± 43	0.000031 ± 0.00001	25400	0 0004
WT	78 6 ± 41	0.000029 ± 0 000007	35300	0 0003
dG-dTTP				
D63P	34.5 ± 12	0 0010 ± 0.0007	793	0 001
WT	58.8 ± 20	0.0039 ± 0 0017	240	0 004

Error frequencies and fidelities were calculated from catalytic efficiencies for correct and incorrect nucleotide insertion, fidelity = error frequency $^{-1}$ = $[(k_{cat}/K_m)_{correct}+(k_{cat}/K_m)_{incorrect}]/(k_{cat}/K_m)_{incorrect}$

Chapter 4

DISCUSSION

In this study, a mutant of *X*polβ was formed at residue 63 by changing the native aspartic acid to proline. The *X*polβ mutant protein mimics the human amino acid sequence at position 63. Residue 63 is located within the hairpin of a helix-hairpin-helix (HhH) motif in human Polβ as resolved by X-ray crystallography [3]. HhH motifs have been implicated in DNA-protein binding. Steady-state kinetic assays were performed to study fidelity of the D63P mutant in comparison to native *X*polβ. Assuming the HhH motif is involved in protein-DNA binding, and that the rate-limiting step of the enzyme is the binding of the DNA to the enzyme, the expectation would be that a change of aspartic acid to proline may modify the enzyme's affinity for the DNA molecule. The primary structure change of the native aspartic acid to a proline residue was expected to change the secondary structure by adding a bend in the structure due to the cyclization of the proline. The change in secondary structure might alter the protein binding constants.

Previous conclusions about the mechanism of human Polβ were based upon calculations of the difference in Gibb's free energy constants. The Gibb's free energy constants were based upon the stability of bonding between correct and incorrect nucleotide arrangements. Fidelity based solely upon the 1-3 kcal/mol difference that is

observed in the bond stability of correct compared to incorrect nucleotide binding, with no discrimination from human Polβ would result in a calculated 10-150 correct incorporations per a single incorrect incorporation. Fidelities for Polβ have been reported at varying ranges from 2,100-14,000 (rat Polβ) [31], 1,900-14,000 (chicken Polβ) [31], and 8,700-245,000 (human Polβ) [31, 32], where fidelity indicates the number of correct incorporation events per single incorrect incorporation event. Fidelity was obtained through a ratio of the catalytic efficiencies in this study (Equation 3-1, page 36). Higher fidelities indicate that polβ makes the incorporation process less susceptible to incorrect incorporation.

Describing the nature of the discrimination of the dNTP substrate in polymerase activity has been approached in two ways, theoretical calculations and calculations based upon studies of independent incorporation reactions. Theoretical calculations have taken into consideration varying parameters which include bond energy, spatial arrangement, and pathway analysis. The 1-3 kcal/mol incorporation difference in bond energy between incorrect and correct bond arrangements took into consideration the differences in the hydrogen bond formation alone with no added polymerase. Other calculations have been made for human polβ according to crystallography images that have considered the spatial arrangement of the incoming dNTP [33]. The dG-gapped substrate possessed the most stable non Watson-Crick base pairing based upon spatial and binding energy. The dG-dTTP base pairing was calculated to have 0.9 kcal/mol difference in the binding energy from the correct base pairing [33].

In this study the steady-state kinetic data from the dG and dT substrate compared catalytic efficiencies of the correct incorporations to incorrect incorporations.

Measurements were made for individual substrate incorporation into the 15-mer gapped template.

dG-gapped template

Correct incorporation of the dG-gapped template's Lineweaver-Burke plot displayed D63P K_m to be similar to WT K_m and the D63P V_{max} to be similar to the WT V_{max}. The compiled results show the dG-gapped template when incorporating dCTP for the D63P K_m is 0.98μM and WT K_m is 1.44μM. For the dG-gapped template when incorporating dCTP substrate the catalytic efficiency for D63P is $0.82\mu M^{-1}s^{-1}$ and WT is $0.93\mu M^{-1}s^{-1}$. Data suggests that the mutant D63P is similar to native protein activity. Analysis of the incorrect incorporation of dATP into the dG-gapped template's Lineweaver-Burke plot shows both similar K_m and V_{max}. The compiled results show the dG-gapped template when incorporating dATP for the D63P K_m is 103.5μM and WT K_m is 78.6μM. For the dG-gapped template when incorporating dATP substrate the catalytic efficiency for D63P is $3.1 \times 10^{-5}\mu M^{-1}s^{-1}$ and WT is $2.9 \times 10^{-5}\mu M^{-1}s^{-1}$. Enzyme binding of the substrate has decreased two orders of magnitude from the correct incorporation. This result supports previous studies finding that the enzyme does have diminished activity between the correct and incorrect base pairing. The increase in K_m also indicates that the enzyme must be at a higher concentration of substrate before the reaction may proceed. The binding of an incorrect nucleotide increases the K_m and decreases the V_{max} of both the D63P mutant and WT enzyme. The catalytic efficiency decreased by five orders of magnitude for both the D63P and WT enzymes. The calculated fidelity from this study would indicate the discrimination of dNTP without any competitive interaction. Fidelity

for incorporation of dATP into the dG-gapped template is 1 in 25,400 and 1 in 35,300 for D63P and WT, respectively. The highest fidelity was observed for dATP incorporation into dG-gapped template. The diminished efficiency of dATP is of interest when considering what is commonly referred to as the "dA rule" [34, 35]. The "dA rule" implies that dATP is the preferred nucleotide to be inserted into DNA when template DNA cannot be established. The increase in fidelity might indicate extra protection of Polβ against added incorrect incorporation of dATP.

Incorrect incorporation of dTTP into the dG-gapped template's Lineweaver-Burke plot shows a lower K_m and a higher V_{max} for D63P in comparison to the WT enzyme. The compiled results show the dG-gapped template when incorporating dTTP for the D63P K_m is 34.5μM and WT K_m is 58.8μM. For the dG-gapped template when incorporating dTTP substrate the catalytic efficiency for D63P is $1.0 \times 10^{-3} \mu M^{-1} s^{-1}$ and WT is $3.9 \times 10^{-3} \mu M^{-1} s^{-1}$. A threefold increase in the catalytic efficiency was observed. Fidelity of D63P is 1 incorrect in 793 correct incorporations and WT is 1 incorrect in 240 correct incorporations. The rise in fidelity of the mutant D63P suggests that the native protein is less efficient distinguishing between the correct and incorrect nucleotide. Methylation of dCTP at C5 produces 5-methylcytosine, whose deamination forms dTTP. This connection of dTTP and dCTP and the threefold increase in fidelity when the protein was altered toward the human form raises suspicion about the role of methylation in *Xiphophorus*. Methylation has been implicated in the activity of gene regulation, DNA/histone packing, and oncogenesis. Within *Xiphophorus* the study of 5-methylcytosine patterns, results have shown that parental methylation patterns are stable in progeny [36]. The methylation pattern at CCGG ("CpG islands") was studied through

the use of MspI (a restricition enzyme used to cleave methylated CCGG sites) [34]. In human development methylation has been hypothesized to regulate gene selection. Human studies have shown that one stage in development is the demethylation of all genomic DNA followed by DNA methylation. The DNA remethylation is thought to select for expressed genes. The observation of a higher fidelity in the mutant *X*polβD63P may suggest *X*polβ is more lenient in protecting against methylation. Further study of the incorporation of 5-methylcytosine and uracil may be undertaken to determine the role of *X*polβ in DNA methylation.

dT-gapped template

Results show the dT-gapped template when incorporating dATP for the *X*polβD63P K_m is 0.19 μM and WT K_m is 0.35 μM. For the dT-gapped template when incorporating dATP substrate the catalytic efficiency for *X*polβD63P is $4.1\mu M^{-1}s^{-1}$ and WT is $3.5\mu M^{-1}s^{-1}$. The low K_m correlates into the incorporation of dATP into the dT-gapped template being the most efficient incorporation of the substrates tested. The dATP substrate was found to be both the most active correct incorporation and the most inactive incorrect incorporation. Purines are bulky in comparison to prymidines. The bulk of dATP might cause limitation in spatial arrangement in the active site. The limitation while restricting multiple bond conformations in the active site also could induce fit when base pairing with the correct dT-gapped template.

Results show the dT-gapped template when incorporating dCTP for the *X*polβD63P K_m is 22.8μM and WT K_m is 54.2μM. For the dT-gapped template when incorporating dCTP substrate the catalytic efficiency for *X*polβD63P is $2.8 \times 10^{-2}\mu M^{-1}s^{-1}$

and WT is 3.8 x $10^{-2}\mu M^{-1}s^{-1}$. Results show the dT-gapped template when incorporating dGTP for the D63P K_m is 13.3μM and WT K_m is 6.6μM. For the dT-gapped template when incorporating dGTP substrate the catalytic efficiency for *X*polβD63P is 5.3 x 10^{-2} $\mu M^{-1}s^{-1}$ and WT is 6.7 x $10^{-2}\mu M^{-1}s^{-1}$. Incorporation of both dCTP and dGTP into the dT-gapped substrate occurred more efficiently than previous fidelity studies. Catalytic efficiency of dGTP is two fold larger than the dCTP substrate. Fidelity of dCTP incorporation into dT-gapped template is 147 and 92 for *X*polβD63P and WT *X*polβ, respectively. Fidelity of dGTP incorporation into dT-gapped template is 78 and 53 for D63P and WT, respectively. Efficiencies of nucleotides of like size to the correct nucleotide (ex. dGTP and dATP or dCTP and dTTP) might indicate that size plays a large role into the coordination of the enzyme-template-substrate complex.

dA-gapped template

The dA-gapped template shows that D63P K_m to be greater than WT K_m and the D63P V_{max} to be higher than the WT V_{max}. Results show the dA-gapped template when incorporating dTTP for the D63P K_m is 1.21μM and WT K_m is 0.75μM. For the dA-gapped template when incorporating dTTP substrate the catalytic efficiency for D63P is $1.4\mu M^{-1}s^{-1}$ and WT is $1.6\mu M^{-1}s^{-1}$. The overall functionality of the protein was unaltered for the correct incorporation into the dA-gapped template.

dC-gapped template

The dC-gapped template shows that D63P K_m to be greater than WT K_m and the D63P V_{max} to be similar to the WT V_{max}. The compiled results show the dC-gapped

template when incorporating dGTP for the D63P K_m is 0.97μM and WT K_m is 0.41μM. For the dC-gapped template when incorporating dGTP substrate the catalytic efficiency for D63P is $1.3\mu M^{-1}s^{-1}$ and WT is $2.1\mu M^{-1}s^{-1}$. D63P in this case has an increase in K_m. D63P in this situation would require the presence of more substrate before binding at full potential. The catalytic efficiency also displays D63P as less efficient in inserting dGTP into the dC-gapped template.

In a previous study of *Xiphophorus* Polβ all fidelities were greater than 1 in 610 incorporations [23]. Interpretation of the results from the previous study also indicated that some additional mechanism was in place for discrimination against incorrect nucleotide incorporation. In this previous study enzyme reactions for fidelity were conducted at a temperature of 37°C while herein reaction temperatures were held at 15°C, the *Xiphophorus* optimal activity temperature [23]. Data shown in table 3-1 suggests that the additional selectivity mechanism provided by the enzyme is more prominent with dG gap template and the enzymatic efficiency in incorrect incorporations is lower at higher temperatures and the overall velocity decreases with an increase in temperature in the *Xiphophorus* model. The results herein compared with those of the previous *Xiphophorus* Polβ study would suggest that with a decrease in reaction temperature the enzymes in this study function through a less discriminating mechanism.

In a study of the human Polβ, a mutant T79S, that is located within the same domain as the *X*polβ D63P variant was tested to examine enzyme fidelity. The human Polβ T79S mutation is positioned between the two HhH motifs in the 8 kDa thumb domain. There were no data presented for the human Polβ T79S mutant with a dG-gapped template, however data was provided for a single-nucleotide dT-gapped template.

The incorrect incorporation of dGTP into the dT-gapped template with the mutant was found to enhance fidelity by two fold [24]. In our study, the incorporation of dGTP into the dT-gapped template for *X*polβD63P also displayed an increase in fidelity by two fold. The human Polβ T79S mutant study also examined the pre-steady state kinetics of the enzyme. The pre-steady state kinetics showed the rate-determining step of the incorrect incorporation reaction for the human Polβ T79S mutant was shifted to a step after phosphodiester bond formation compared to the wild-type human Polβ [24]. It was suggested that after phosphodiester bond formation the human Polβ T79S mutant had a greater affinity for the DNA strand and thus had difficulty releasing the DNA product. Future study of *X*polβD63P may involve the analysis of the pre-steady state kinetics. Interestingly the human Polβ T79S mutant showed an increase in mutation rate when the substrate was changed from the single-nucleotide gapped substrate to a 3′ recessed DNA substrate. Further study on *X*polβD63P may involve the incorporation of incorrect nucleotides into a 3′ recessed DNA substrates. The human Polβ T79S implicates HhH involvement in both the DNA binding and in positioning of the substrates in the active site. The combination of a pre-steady state kinetic study and the alternative substrate interactions observed for *X*polβD63P may yield a more encompassing view of the role of the hairpin within the HhH motif.

Studies of other variants of the *X*polβ enzyme, such as F18M and the N30SR31Q, have been initiated in our laboratory. The study of the variation of proteins across species has been undertaken in an effort to understand the structure-function relations within homologous enzymes.

As mentioned, previous study of *X*polβ examined the difference of correct

insertion activity at varying temperatures in comparison with the human Polβ. Studies presented were obtained at the optimal temperature for the *X*polβ [23]. The temperature of the nucleotide incorporation activity assay was altered from the previous study 37°C to 15°C. With the change of temperature a change in the preference of correct nucleotide was observed. To ascertain the temperature effect upon the incorporation of nucleotides and also the incorporation of incorrect nucleotides more assays using varying temperatures would be needed. Appearance of a change in selectivity may occur due to limitation of space and enzyme condensation or expansion of the active site as temperature is decreased. Also, environments with varying concentrations of certain salts may be of some interest to find optimal *X*polβ activity as *Xiphophorus* may have a different intracellular ionic environment compared to other species studied [37, 38].

Works Cited

[1] Pelletier, H., 1994. Polymerase Structures and Mechanism. *Science* 266: 2025-2026.

[2] Kraynov, V. S., Showwalter, A., Liu, J., Zhong, X., and Tsai, M., 2000. DNA polymerase B: contributions of template-positioning and dNTP triphosphate-binding residues to catalysis and fidelity. *Biochemistry* 39: 16008-16015.

[3] Pelletier, H., Sawaya, M., Wolfe, W., Wilson, S., and Kraut, J., 1996. Crystal structures of human DNA polymerase B complexed with DNA: implications for catalytic mechanism, processivity, and fidelity. *Biochemistry* 35: 12742-12761.

[4] Tanabe, K., Bohn, E. W., and Wilson, S., 1979. Steady-state Kinetics of Mouse DNA Polymerase-beta. *Biochemistry* 18: 3401-3406.

[5] Sawaya, M., Prasad, R., Wilson, S., Kraut, J., and Pelletier, H., 1997. Crystal structures of human DNA polymerase B complexed with gapped and nicked DNA: evidence for an induced fit mechanism. *Biochemistry* 36: 11205-11215.

[6] Schlick, T., Radhakrishnan, R., 2004. Orchestration of cooperative events in DNA synthesis and repair mechanism unraveled by transition path sampling of DNA polymerase B's closing. *Proceedings of the National Academy of Science* 16: 5970-5975.

[7] Pelleitier, H. and Sawaya, M., 1996. Characterization of the metal ion binding helix-hairpin-helix motifs in human DNA polymerase B by X-Ray structural analysis. *Biochemistry* 35: 12778-12787.

[8] Wong, I., Patel, S., and Johnson, K., 1991. An induced-fit kinetic mechanism for DNA replication fidelity: direct measurement by single-turnover kinetics. *Biochemistry* 30: 526-537.

[9] Sokhansanj, B., Rodrigue, G., Fitch, J .P., and Wilson III, D., 2002. A quantitative model of human DNA base excision repair. I. Mechanistic insights. *Nucleic Acids Research* 30(8): 1817-1825.

[10] Lindhal, T., 1993. Instability and decay of the primary structure of DNA. *Nature* 362: 709-715.

[11] Matsuda, T., Berg, B., Bebeneck, K., Osheroff, W., Wilson, S., and Kunkel, T., 2000. The base substitution fidelity of DNA polymerase β-dependent single nucleotide base excision repair. *The Journal of Biological Chemistry* 278(28): 25947-25951.

[12] Bennett, R., Wilson III, D., Wong, D, and Demple, B., 1997. Interaction of human apurinic end nuclease and DNA polymerase β in the base excision repair pathway. *Proceedings of the National Academy of Science* USA 94: 7166-7169.

[13] Dimitriadis, E., Prasad, R., Vaske, M., Chen, L., Tomikinson, A., Lewis, M., and Wilson, S., 1998. Thermodynamics of human DNA ligase I dramatization and association with DNA polymerase B. *The Journal of Biological Chemistry* 273(32): 20540-20550.

[14] Kedar, P., Kim, S., Robertson, A., Hou, E., Prasad, R., Horton, J., and Wilson, S., 2002. Direct interaction between mammalian DNA polymerase β and proliferating cell nuclear antigen. *The Journal of Biological Chemistry* 277: 31115-31123.

[15] Ahn, J., Kraynov, S., Zhong, X., Werneburg, B., Tsai, M., 1997. DNA polymeraseβ: effects of gapped DNA substrates on dNTP specificity, fidelity, processivity, and conformational changes. *Journal of Biochemistry* 331: 79-87.

[16] Sugo, N., Aratani, Y., Nagashima, Y., Kubota, Y., and Koyama, H., 2000. Neonatal lethality with abnormal neurogenesis in mice deficient in DNA polymerase β. *EMBO Journal* 19(6): 1397-1404.

[17] Gu,H., Marth, J., Orban, P., Mossmann, H., and Rajewsky, K., 1994. *Science* 265: 103-106.

[18] Walter, R., 2001. Introduction: aquaria fish models of human disease. *Marine Biotechnology* 3: S1-S2.

[19] Nairn, R., Kazianis, S., Coletta, L., Trono, D., Butler, A., Walter, R., and Morizot, D., 2001. Genetic analysis of susceptibility to spontaneous and uv-induced carcinogenesis in *Xiphophorus* hybrid fish. *Marine Biotechnology* 3: S24-S36.

[20] Kazianas, S., Conti, I., Setlow, R., Woodhead, A., Harshbarger, J., Trono, D., Ledesma, M., Nairn, R., and Walter, R., 2001. MNU induction of neoplasia in a platyfish model. *Laboratory Investigation* 81(9): 1191-2001.

[21] Vielkind, J. R., Kallman, K. D., Morizot, D. C., 1989. *Journal of Aquatic Animal Health* 1: 69-77.

[22] Schwab, M., Abdo, S., Ahuja, M. R., Kollinger, G., Anders, A., Anders, F., and Frese, K., 1978. *Cancer Research Clinical Oncology*, 91: 301-315.

[23] Oehlers, L., Heater, S., Rains, D., Wells, M., and Walter, R., 2004. Gene structure, expression and characterization of DNA polymerase β from *Xiphophorus maculatus*. *Comparative Biochemistry and Physiology*, Part C 138: 311-324.

[24] Maitra, M., Gudzelak, A., Li, S., Matsumoto, Y., Eckert, K., Jager, J., and Sweasy, J., 2002. Threonine 79 is a hinge residue that governs the fidelity of DNA within the active site. *The Journal of Biological Chemistry* 277(38): 35550-35560.

[25] Reichenberger, S., and Pfieffer, P., 1998. Cloning, Purification, and characterization of DNA Polymerase β from *Xenopus laevis*. *European Journal of Biochemistry* 251: 81-90.

[26] Abbotts, J., SenGupta, D., Zmudzka, B., Widen, S., Notario, V., and Wilson, S., 1988. Expression of human DNA polymerase β in *Escherichia coli* and characterization of the recombinant enzyme. *Biochemistry* 27: 901-909.

[27] Date, T., Yamaguchi, M., Hirose, F., Nishimoto, Y., Tanihara, K., and Matsukage, A., 1988. Expression of active DNA polymerase β in *Escherichia coli*. *Biochemistry* 27: 2983-2990.

[28] Wong, I., Patel, S. S., and Johnson, K. A., 1991. An induced-fit kinetic for DNA replication fidelity: direct measurement by single-turnover kinetics. *Biochemistry* 30: 526-537.

[29] Beard, W. A, Shock, D. D., Yang, X. P., DeLauder, S. F., and Wilson, S. H., 2002. Loss of DNA polymerase β stacking interactions with purines, but not pyrimidines, alters catalytic efficiency and fidelity. *Journal of Biological Chemistry* 277: 8235-8242.

[30] Johnson, K. A., 1993. Conformational coupling in DNA polymerase fidelity. *Annual Review in Biochemistry* 62: 685-713.

[31] Kunkel, T. and Loeb, L., 1979. On the fidelity of DNA replication. *Journal of Biological Chemistry* 254: 5718-5725.

[32] Werneburg, B. G., Ahn, J., Zhong, X., Hondal, R. J., Kraynov, V. S., and Tsai, M., 1996. DNA polymerase β: pre-steady-state kinetic analysis and roles of arginine-283 in catalysis and fidelity. *Biochemistry* 35(22): 7041-7050.

[33] Florian, J., Goodman, M., and Warshel, A., 2003. Computer simulation studies of the fidelity of DNA polymerases. *Biopolymers* 68: 286-299.

[34] Goodman, M., Creighton, S., Bloom, and L., Putruska, J., 1993. Biochemical basis of DNA replication. *Critical Review of Biochemical Molecular Biology* 28: 83-126.

[35] Strauss, B., 1991. The "A Rule" of mutagen specificity: a consequence of DNA polymerase bypass of non-instructional lesions? *Bioessays* 13: 79-84.

[36] Li, H., Savage, T., Obermoeller, R., Kazianis, S., and Walter, R., 2002. Parental 5-methylcytosine methylation patterns are stable upon interspecies hybridization of *Xiphophorus* (*Teleostei: Poeciliidae*) fish. *Comparative Biochemistry and Physiology*, Part B 133: 581-595.

[37] Schartel, M., 1995. Platyfish and swordtails: a genetic system for the analysis of molecular mechanisms in tumor formation. *Trends in Genetics* 11(5).

[38] Kallman, K. D., 1975. The Platyfish, *Xiphophorus maculatus*. *Handbook of Genetics*, Vol. 4, Edited by R.C. King. Plenum Publishing Company, New York: p. 81-132.

VITA

Douglas Barth was born in Austin, Texas, on March 15, 1980 the son of Roy Barth and Nikki Barth. After completing his work at San Marcos High School, San Marcos, Texas in 1998, he entered Baylor University. He received the degree of Bachelor of Science from Baylor University in December 2002. In January 2003, he entered Texas State University-San Marcos.

Permanent Address: 602 Quail Run

San Marcos, Texas 78666

This thesis was typed by Douglas Barth.